Rajani, V., Zhang, Y., Jalubula, V., Rancic, V., Sheikhbahaei, S., Zwicker, J. D., Pagliardini, S., Dickson, C. T., Ballanyi, K., Kasparov, S., Gourine, A. V., & Funk, G. D. (2017). Release of ATP by pre-Bötzinger complex astrocytes contributes to the hypoxic ventilatory response via a Ca^{2+}-dependent $P2Y_1$ receptor mechanism. *Journal of Physiology*. https://doi.org/10.1113/JP274727

Release of ATP by preBötzinger Complex astrocytes contributes to the hypoxic ventilatory response via a Ca^{2+}-dependent $P2Y_1$ receptor mechanism

Abbreviated title: O_2 homeostasis: ATP and the preBötzinger Complex

Rajani V[1*], Zhang Y[1], Jalubula V[1], Rancic V[1], SheikhBahaei S [2,5], Zwicker JD[1], Pagliardini S[1], Dickson CT[3], Ballanyi K[1], Kasparov S[4], Gourine AV[5], Funk GD[1#]

[1]Department of Physiology, Neuroscience and Mental Health Institute (NMHI), Women and Children's Health Research Institute (WCHRI), Faculty of Medicine and Dentistry, University of Alberta, Edmonton, Alberta, T6G 2E1, Canada

[2]Cellular and Systems Neurobiology Section, National Institute of Neurological Disorders and Stroke (NINDS), National Institutes of Health (NIH), Bethesda, Maryland, 20892, USA

[3]Department of Psychology, Neuroscience and Mental Health Institute (NMHI), Faculty of Science, Edmonton, Alberta, T6G 2E9, Canada

[4]Department of Physiology, Pharmacology and Neuroscience, University of Bristol, Bristol, BS8 1TD, UK

[5] Centre for Cardiovascular and Metabolic Neuroscience, Neuroscience, Physiology & Pharmacology, University College London, London, WC1E 6BT, UK

[*]Current Affiliation: Neurosciences & Mental Health, Peter Gilgan Centre for Research and Learning (PGCRL), The Hospital for Sick Children, Toronto, Ontario, M5G 0A4, Canada

[#]Corresponding Author:
G.D. Funk
3-020G Katz Group Centre, Department of Physiology
University of Alberta, Edmonton, Alberta
Canada, T6G 2E1
Phone: 1-780-492-8330 FAX: 1-780-492-8915
Email: gf@ualberta.ca

Number of pages: 44
Number of figures: 12
Number of tables: 0

KEY POINTS SUMMARY

- The ventilatory response to reduced oxygen (hypoxia) is biphasic, comprising an initial increase in ventilation followed by a secondary depression.
- Our findings indicate that during hypoxia in vivo, astrocytes in the pre-Bötzinger Complex (preBötC), a critical site of inspiratory rhythm generation, release a gliotransmitter that acts via the $P2Y_1$ subtype of ATP receptor to increase ventilation and reduce the secondary depression.
- In vitro analyses reveal that ATP excitation of the preBötC involves $P2Y_1$ receptor-mediated release of Ca^{2+} from intracellular stores.
- By identifying a role for gliotransmission and the sites, P2 receptor subtypes, and signaling mechanisms via which ATP modulates breathing during hypoxia, these data advance understanding of mechanisms underlying the hypoxic ventilatory response and highlight the significance of purinergic signalling and gliotransmission in homeostatic control.
- Clinically, these findings are relevant to conditions in which hypoxia and respiratory depression are implicated including apnea of prematurity, sleep disordered breathing, and congestive heart failure.

ABSTRACT

The hypoxic ventilatory response (HVR) is biphasic, consisting of a phase I increase in ventilation followed by a secondary depression (to a steady-state phase II) that can be life-threatening in premature infants who suffer frequent apneas and enhanced respiratory depression. ATP released in the ventrolateral medulla during hypoxia attenuates the secondary depression. We explored our working hypothesis that vesicular release of ATP by astrocytes in the preBötzinger Complex (preBötC) inspiratory rhythm generating network acts via $P2Y_1$ receptors to mediate this attenuation. Blockade of vesicular exocytosis in preBötC astrocytes bilaterally (using an adenovirus to specifically express tetanus toxin light chain (TeLC) in astrocytes) reduced the HVR in anesthetized rats,

indicating that exocytotic release of a gliotransmitter contributes to the hypoxia-induced increase in ventilation. Unilateral blockade of $P2Y_1$ receptors via local antagonist injection caused an increased secondary depression, revealing that a significant component of the phase II increase in ventilation in vivo is mediated by ATP acting at $P2Y_1$ receptors within the preBötC. In vitro responses of the preBötC inspiratory network, preBötC inspiratory neurons and cultured preBötC glia to purinergic agents indicate that the $P2Y_1$ receptor-mediated increase in fictive inspiratory frequency involves release of Ca^{2+} from intracellular stores and thapsigargin-sensitive increases in intracellular Ca^{2+} ($[Ca^{2+}]_i$) in inspiratory neurons and glia. These data suggest that ATP is released from preBötC astrocytes during hypoxia and acts via $P2Y_1$ receptors on inspiratory neurons (or glia) to evoke Ca^{2+} release from intracellular stores and an increase in ventilation that counteracts the hypoxic respiratory depression.

Abbreviations. AP5, D-(-)-2-amino-5-phosphonopentanoic acid; AVV, adenoviral vector; BME, basal medum Eagle; CNQX, 6-cyano-7-nitroquinoxaline-2,3-dione; CPA, cyclopiazonic acid; DLH, DL-homocysteic acid; eGFP, enhanced green fluorescent protein; GFAP, glial fibrillary acidic protein; GPCR, g-protein coupled receptor; HVR, hypoxic ventilatory response; IP_3, inositol triphosphate; NTS, nucleus tractus solitarius; PKC, protein kinase C; PLC, phospholipase C; PNA, phrenic nerve amplitude; preBötC, preBötzinger Complex; SERCA, sarco/endoplasmic reticulum Ca^{2+}-ATPase; SP, substance P; TeLC, tetanus light chain; TMPAP, transmembrane prostatic acid phosphatase; V_E, minute ventilation; VLM, ventrolateral medulla; V_T, tidal volume.

INTRODUCTION

Acute exposure of mammals to moderate hypoxia evokes a biphasic hypoxic ventilatory response (HVR), comprising an initial increase in ventilation within the first minute followed by a secondary depression to a lower steady-state (Moss, 2000). The initial, phase I increase is primarily attributed to activation of the carotid body chemoreceptors. The secondary depression to a lower steady-state, phase II level is largely

central in origin (Teppema & Dahan, 2010), is implicated in cardiovascular diseases that accompany obstructive sleep apnea (Horner, 2012), and may also be a factor in sudden explained death in epilepsy (So, 2008). Interestingly, the HVR changes developmentally. In adults, ventilation during phase II remains above baseline. Newborn mammals experience a similar phase I increase in ventilation but this is followed by a much larger respiratory depression during which ventilation falls below baseline (Moss, 2000). As a result, infants who suffer from apnea of prematurity experience frequent apneas that can lead to a life-threatening positive feedback loop in which apnea causes hypoxia leading to respiratory depression and greater hypoxia. Despite its clinical significance, underlying mechanisms are poorly understood, reflecting, in part, variability in the severity of hypoxic stimulus used to study the HVR, as well as developmental and species differences in the magnitude of the depression and its underlying mechanisms (Funk, 2013).

A role for ATP-mediated purinergic signaling in shaping the HVR is supported by data showing the release of ATP at the ventrolateral medullary surface and an enhanced secondary respiratory depression following application of P2 receptor antagonists to the ventral medullary surface in vivo (Gourine *et al.*, 2005). In the in vitro rhythmic slice preparation, the activation of P2 (specifically $P2Y_1$) receptors in the preBötzinger Complex (preBötC, a key site of inspiratory rhythm generation) produces a robust 2-4 fold increase in the frequency of fictive inspiratory burst activity (Lorier *et al.*, 2007). Additionally, unanesthetized rats transfected to express transmembrane prostatic acid phosphatase (TMPAP, a potent ectonucleotidase) in the ventrolateral medulla (VLM) to reduce endogenous levels of extracellular ATP, or tetanus toxin light chain (TeLC) protein to block vesicular release specifically in astrocytes, exhibit a decreased HVR. Astrocytes are the likely source of ATP, because they have a mitochondria-based hypoxia sensing mechanism that can evoke vesicular release of ATP (Angelova *et al.*, 2015). These data suggest that the exocytotic release of ATP from astrocytes contributes directly to the homeostatic hypoxic ventilatory response (Angelova *et al.*, 2015). The sites and mechanisms via which ATP causes ventilation to increase during hypoxia remain to be determined. Our working model, depicted in Fig. 1., proposes that preBötC astrocytes sense reductions in O_2 and respond by releasing calcium from intracellular stores (i), which

evokes exocytotic release of gliotransmitters, including ATP (ii). ATP then activates $P2Y_1$ receptors located on preBötC inspiratory neurons (iii), which leads to phospholipase C mediated release of calcium from intracellular stores (iv), and the modulation of downstream ion channels via DAG/IP3 or the activation of protein kinase C (PKC) (v).

Within this framework, we first examined the role of gliotransmission in the phase I and II components of the HVR using a viral approach to disrupt vesicular release specifically within astrocytes of VLM in anesthetized, vagotomized adult rats. Second, based on data from rhythmically-active brainstem slices (Funk *et al.*, 1997; Lorier *et al.*, 2004; Lorier *et al.*, 2007; Lorier *et al.*, 2008; Huxtable *et al.*, 2009; Zwicker *et al.*, 2011) that ATP excitation of the preBötC is mediated via $P2Y_1$ receptors, we tested in anesthetized rats in vivo whether ATP released during hypoxia acts in the preBötC via $P2Y_1$ receptors to increase ventilatory output and attenuate the secondary depression. Finally, $P2Y_1$ receptors on neurons and astrocytes in other brain regions signal primarily through the $G\alpha_{q/11}$ G-protein coupled receptor (GPCR) pathway to activate PLC and IP_3-mediated Ca^{2+} release from intracellular stores (Simon *et al.*, 1995; von Kugelgen & Wetter, 2000; Sak & Illes, 2005), which modulates neuronal excitability or transmitter release through $[Ca^{2+}]_i$-dependent signalling. To assess the role of the $G\alpha_{q/11}$ signaling pathway in mediating the excitatory actions of $P2Y_1$ receptors on the preBötC network, we used rhythmic medullary slices from neonatal rats to compare the effects of $P2Y_1$ receptor activation on: i) the network response before and after chelating intracellular calcium and inhibition of sarco/endoplasmic reticulum Ca^{2+} ATPase (SERCA), and ii) the calcium response evoked in inspiratory neurons and preBötC glia by $P2Y_1$ receptor activation before and after SERCA inhibition. These data advance our understanding of the sites, receptor mechanisms and signaling cascades that underlie the contribution of astroglial purinergic signaling to the HVR.

METHODS

All the experiments were performed in accordance with the guidelines of the Canadian Council on Animal Care and European Commission Directive 2010/63/EU

(European Convention for the Protection of Vertebrate Animals used for Experimental and Other Scientific Purposes) with project approval from the respective Institutional Animal Care and Use Ethics Committees.

Preparations

Adult in vivo preparations

Adult male Sprague-Dawley rats (250-350 g) were anesthetized using isofluorane (3% in 100% O_2) and the femoral vein was cannulated. Isofluorane anesthesia was then replaced with urethane (1.5-1.7 g/kg) delivered intravenously (i.v.). Additional doses of urethane were given as necessary. The femoral artery was cannulated to monitor arterial blood pressure (BP) and blood gases. The trachea was cannulated, and the vagus nerves resected bilaterally at the mid-cervical level to eliminate confounding effects of vagal reflex stimulation. From this point there were two variations of the preparation.

For hypoxia experiments, animals were paralyzed with gallamine triethoiodide or pancuronium bromide (10 mg/kg i.v.; 1 mg/kg) and mechanically ventilated with a mix of 20% or 30% O_2, balance N_2 (1 L/min, 60 strokes/min at ~2 ml/stroke, for a tidal volume of 8 ml/Kg). Paralysis and pump ventilation were used to open chemoreflex loops so that changes in central respiratory drive would not affect blood gases. End-tidal O_2 and CO_2 were monitored from a small port in the tracheal tube (PowerLab gas analyzer, ML206, AD Instruments, Colorado Springs, CO) to ensure that end-tidal CO_2 remained constant. Blood gases were taken before and during the hypoxic challenges to ensure that arterial PO_2, PCO_2, and pH were within physiological ranges and consistent between control and experimental trials.

Once the rat was placed in prone position in a stereotaxic device (Kopf Instruments, Tujunga, CA), and mechanically ventilated, the brachial plexus was exposed dorsolaterally behind the right shoulder blade. The phrenic nerve was isolated, cut distally, placed over dual platinum electrodes and embedded in kwik-sil adhesive (World Precision Instruments, Sarasota, FL) for long-term stability and to prevent nerve desiccation.

Experiments that tested the acute effects of locally applying purinergic agonists into the preBötC were conducted in spontaneously breathing animals. Electrodes made from

Teflon-coated wires (AM Systems, Carolsborg, WA) were placed in the genioglossus and diaphragm muscles to record electromyographic activity (GG_{EMG} and $DIA_{EMG,}$ respectively). The animal was then positioned in a stereotaxic frame in prone position. Body temperature was maintained at 37°C in all in vivo experiments with a servo-controlled heating pad (Harvard Apparatus, Holliston, MA).

Rhythmically-active medullary slice preparation

Rhythmically-active medullary slices were obtained from neonatal rats (P0-P4) as described in detail previously (Smith *et al.*, 1991; Ruangkittisakul *et al.*, 2006; Zwicker *et al.*, 2011). Briefly, rats were anesthetized through inhalation of isofluorane and decerebrated. The brainstem spinal cord was then isolated in cold artificial cerebrospinal fluid (aCSF) containing (in mM): 120 NaCl, 3 KCl, 1.0 $CaCl_2$, 2.0 $MgSO_4$, 26 $NaHCO_3$, 1.25 NaH_2PO_4, 20 D-glucose, and bubbled with 95% O_2 – 5% CO_2. The brainstem-spinal cord was pinned to a wax chuck, and serial 100-200 μm sections were cut in the rostral to caudal direction using a vibrating microtome (VT1000S, Leica, Nussloch, Germany). Sections were trans-illuminated to identify anatomical landmarks. The structure of the subnuclei of the inferior olive was particularly useful in defining this boundary. A 700 μm rhythmic transverse slice containing the preBötC was obtained. Special care was made to ensure that the preBötC was at the rostral surface of the slice (~0.35mm caudal to the caudal aspect of the facial nucleus) (Smith *et al.*, 1991; Ruangkittisakul *et al.*, 2006; Lorier *et al.*, 2007; Ruangkittisakul *et al.*, 2008). Rhythmic slices were pinned rostral surface up on Sylgard resin in a 5 ml recording chamber and perfused with aCSF at a flow rate of 15 ml/min (dead space of perfusion system including inflow and outflow lines and chamber was ~20 ml). The concentration of K^+ in the aCSF ($[K^+]_e$) was raised from 3 to 9 mM at least 30 min before the start of data collection to produce prolonged stable rhythm (Ruangkittisakul *et al.*, 2006). Rhythmic slice experiments were conducted at room temperature (23 -24°C).

Primary cultures of glia isolated from the preBötC

Culture preparation. Cultures were prepared from 300 μm thick preBötC slices

from neonatal rats (P0-P4) as described in detail previously (Huxtable et al., 2010). Culture media were used at 37 °C. The preBötC region was collected bilaterally using 21 gauge tissue punches. Tissue punches were transferred to separate 15 ml conical tubes, washed (2×) with Dulbecco's PBS (2 ml) (Invitrogen, Carlsbad, CA), and centrifuged (1500 × g, 1 min). PreBötC tissue was plated directly on Thermanox plastic coverslips (Invitrogen, Carlsbad, CA) and placed in a T25 flask containing BME-glucose (1 ml) that was produced by adding to 1× basal medium Eagle solution (BME; Invitrogen, Carlsbad, CA): 3.3 mM glucose (final concentration of 8.8 mM), 2 mM L-Glutamine (Sigma-Aldrich, St. Louis, MO), penicillin/ streptomycin (10,000 U of penicillin/10,000 μg of streptomycin per ml; (Invitrogen, Carlsbad, CA), and 10% rat serum.

PreBötC-containing coverslips were incubated in 1 ml of BME-glucose for the first 24 h and 1 ml of BME-sorbitol (10% rat serum) thereafter. BME-sorbitol was equivalent to BME-glucose except that D-glucose was replaced with sorbitol (2.5 mM, Fisher Scientific, Waltham, MA) to select for glia. After 48 h, fresh media (with 2.5% rat serum) was added and changed every 3 days. Cultures were grown for 6 days, smeared, maintained in a 24-well plate for 2 weeks and then imaged.

Viral gene transfer in vivo

Adult male rats (200-250 g) were anesthetized with a mixture of ketamine (90 mg/kg i.p.) and xylazine (10 mg/kg, i.p). They were then placed in a stereotaxic frame, where a small craniotomy was performed to expose the obex. Using coordinates described below, adenoviral vectors were injected bilaterally into the preBötC. Glial expression of TeLC and enhanced green fluorescent protein (eGFP) was achieved using a bicistronic adenoviral vector (AVV) construct as previously described, where eGFP expression was linked to TeLC via a "SKIP" sequence (Angelova *et al.*, 2015). The bicistronic construct, making use of the viral ribosomal skipping mechanism, allows for a high expression of eGFP while attenuating TeLC expression to avoid cell toxicity. Vectors contained enhanced shortened GFAP promoter to drive expression of TeLC and eGFP (AVV-sGFAP-eGFP-TeLC). As a control, we used an adenovirus expressing eGFP only (AVV-sGFAP-eGFP).

Viruses were diluted in HEPES buffer, and slowly injected into the preBötC under direct visualization (500 nl over 2 min). Following injection, the pipette remained in place for 5 min before withdrawal. The skin was sutured and the animal was put in post-operative care and closely observed throughout recovery from anesthesia. Rats were left to recover for 6-8 days before the in vivo experiments to ensure stable viral expression. Virus dilution and the post-injection incubation period were established through experiments that involved a series of 10-fold dilutions and incubation periods that varied from 5-9 days. Rats were euthanized at the end of the respective incubation period, perfused and tissue examined to define the dilution and incubation period that provided the strongest glial expression with no evidence of tissue damage. High virus concentrations produced bright yet grainy fluorescent expression and transfected cell bodies near the injection site were hard to locate, consistent with cell death/damage. Low virus concentrations yielded weaker eGFP fluoresence, but individual cell bodies and processes were clearly identifiable. Original viruses of titres 1.4×10^{11} (control) and 2.10×10^{10} (TeLC) were diluted 1:100. Viruses were produced and supplied by Sergey Kasparov at the University of Bristol.

Immunohistochemistry

At the end of the experiments, the rats were perfused transcardially with 10% saline (100 ml), followed by 4% paraformaldehyde (PFA, 100 ml). The brainstem was removed and submersion fixed for at least 24 hours in 4% PFA solution. The brainstems were sectioned serially into 50 μm slices in PBS solution using a vibratome (VT 1000S, Leica, Nussloch, Germany). The preBötC was identified based on anatomical landmarks; ~800 μm caudal to caudal border of the facial nucleus, at the same level as the lateral loop of the principal subnucleus of the inferior olive and the semi-compact nucleus ambiguus, just caudal to compact nucleus ambiguus (Paxinos & Watson, 2007; Ruangkittisakul *et al.*, 2008). The well-established preBötC marker, NK1 receptor immunolabeling, was also used to define the preBötC. Serial sections were examined for the region of most intense labeling indicative of the preBötC (Guyenet & Wang, 2001; Guyenet *et al.*, 2002). MRS 2279 ($P2Y_1$ receptor antagonist) injection sites were identified via fluorescent microspheres (0.1

μm, yellow-green, 2% solids, Life Technologies). NK1 receptor immunolabeling was examined using a rabbit anti-NK1 receptor primary antibody (1:1000, cat#AB-5060, Millipore, Billerica, MA) with a Cy3-conjugated donkey anti-rabbit secondary (1:200, cat# 711-165-152, Jackson ImmunoResearch, West Grove, PA). To assess viral expression, eGFP fluorescence was enhanced with a chicken anti-GFP primary antibody (1:1000, cat# GFP-1020, Aves Labs, Tigard, OR) and an AlexaFluor 488 anti-chicken secondary antibody (cat# A-11039, Life Technologies, Carlsbad, CA). To check glial specificity of viral expression we used Cy3-conjugated NeuN rabbit antibody (1:200, cat# ABN78C3, Millipore) to stain neuronal nuclei. Slices were mounted on slides and observed with a fluorescent microscope (DM5500, Leica, Nussloch, Germany) and a Hamamatsu digital camera. Low magnification images to assess injection site were acquired through MetaMorph (Molecular Devices, Sunnyvale, CA) acquisition software, and the extent of viral expression analyzed using ImageJ (NIH, MD) and Adobe Photoshop (San Jose, CA). High magnification images were taken with a confocal microscope (Leica TCS SP5, Nussloch, Germany) to assess cellular expression patterns. Regions of interest were delineated by identifying NeuN labeled neuronal cell bodies under Cy3 fluorescence and then switching to GFP fluorescence to check for eGFP fluorescence indicative of neuronal expression of virally-transfected protein.

Recording of muscle, nerve, and neuronal activities

In vivo recordings of EMG and phrenic nerve activities were amplified using a differential AC amplifier (model 1700, AM-systems, Sequim WA) and sampled at 2 kHz using a PowerLab 16/30 data acquisition system (AD Instruments Colorado Springs, CO). Phrenic nerve activity was rectified, bandpass filtered (300 Hz to 1 kHz) and the raw signal was integrated (time constant = 0.08s) to calculate respiratory frequency and phrenic nerve inspiratory burst amplitude as an index of central respiratory drive.

In vitro recordings of inspiratory activity were made using glass suction electrodes (AM Systems, Carlsborg, WA) placed on the XII (hypoglossal) nerve rootlets. Inspiratory-related field potentials were also recorded from the surface of the slice using a four-axis

manual manipulator to place a suction electrode (120 μm inside diameter) on the surface of the slice over the rostrally-exposed preBötC (Ramirez *et al.*, 1996). The pipette was systematically moved in 60 μm steps until the most robust signal was detected**.** This technique was used to establish the approximate location of the preBötC to assist local drug injection. Signals were amplified, bandpass filtered (300 Hz to 1 kHz), rectified, integrated and displayed using Axoscope 9.2 (Molecular Devices, Sunnyvale CA, USA). Data were saved using a Digidata 1322 A/D board and Axoscope 9.2 software for offline analysis.

Responses of cultured glia were measured using Fluo-4 Ca^{2+} imaging. Cultures were loaded for 45 min (35°C) with the membrane-permeant Ca^{2+}-sensitive dye, fluo-4-AM (0.01 mM, Sigma-Aldrich, Oakville ON) in aCSF, containing the following (in mM): 117 NaCl, 5 KCl, 1 NaH_2PO_4, 2 $CaCl_2$, 1 $MgSO_4$, 26 $NaHCO_3$, and 6 glucose. Coverslips were then moved to the recording chamber (3 ml volume, 28°C, 6 ml/min flow rate) containing aCSF saturated with 20% O_2, 5% CO_2, 75% N_2. Fluorescence intensity was measured using an upright microscope (Axioskop2 FS Plus, Zeiss, Oberkochen, Germany) fitted with a 40× water-immersion objective (NA = 0.8), xenon arc lamp (175 W, Sutter Instruments, Novato, CA), and a Sensi-Cam QE (PCO Tech, Romulus, MI). Imaging Workbench 6.0 (INDEC Bio- Systems, Santa Clara, CA) was used to control a Lambda 10-2 shutter system (Sutter Instruments, Novato, CA). Images were acquired at 1 Hz (20 ms exposure). Drugs (ATP 10 μM and thapsigargin 50 nM) were applied from triple-barreled micropipettes using a controlled pressure source. Consecutive agonist applications were 10 min apart. The locally-applied ATP concentration was 10-fold lower in these experiments compared to slice experiments because of improved drug access to glial monolayers.

PreBötC inspiratory neuron activity was monitored in rhythmic slices using Fluo-4 Ca^{2+} imaging or whole-cell recording. In calibrated slices (Ruangkittisakul *et al.*, 2006; Ruangkittisakul *et al.*, 2008), the free cytosolic Ca^{2+} concentration ($[Ca^{2+}]_i$) was monitored by Olympus FV1000 MPE multiphoton scanning microscopy. A MaiTai-BB Ti:sapphire femtosecond pulsed laser set to excite at 810 nm was used for fluorescence excitation and an Olympus X 20 1.0 NA immersion objective was used to image the neurons. The membrane-permeant Ca^{2+} dye fluo-4-AM was pressure-injected (25–50 mmHg, 10 min) into the preBötC using a broken patch pipette filled with aCSF containing 0.5 mM Fluo-4-

AM dissolved in dimethyl sulfoxide containing 20% pluronic acid (Sigma Aldrich, Oakville, ON). Neurons and glia, stained in an area of 150–300 μm diameter, were imaged in 30–75 μm depths for several hours at scanning rates of 2.5 Hz that are sufficient to resolve peaks of inspiratory-related $[Ca^{2+}]_i$ rises (for details, see (Ruangkittisakul *et al.*, 2006; Ruangkittisakul *et al.*, 2012).

Whole cell recordings were obtained from preBötC inspiratory neurons in rhythmic slices under direct infrared differential interference contrast microscopy (IRDIC) visualization. A horizontal puller (P-97, Sutter Instruments, Novato, CA) was used to pull patch pipettes from 1.2 mm o.d. filamented borosilicate glass (Harvard Apparatus, Holliston, MA). Pipette resistance was 5.1 ± 0.1 MΩ. The intracellular solution used in this study contained (in mM): 140 potassium gluconate, 5 NaCl, 1 $MgCl_2$, 0.1 EGTA, 10 HEPES, and 1 glucose with pH adjust to 7.25-7.35. Intracellular signals were amplified and filtered (1.8 kHz low-pass Bessel filter) with a MultiClamp 700A amplifier (Molecular Devices, Sunnyvale, CA), acquired at 1 and 5 kHz using a Digidata 1322A A/D board (Molecular Devices, Sunnyvale, CA), for Axoscope 9.2 and Clampex 9.2 (Molecular Devices, Sunnyvale, CA), respectively, and stored to the computer's hard disk for off-line analysis using Clampfit 9.2.

ATP was excluded from the intracellular solution because its inclusion would result in P2 receptor desensitization as solution is pressure ejected from the pipette when approaching the neurons. Recordings were obtained under voltage-clamp conditions at a holding potential of -60 mV. Inspiratory neurons were identified based on the presence of rhythmic inward synaptic current inputs that were synchronized with inspiratory-related bursts recorded from the XII nerve rootlets. Neurons without rhythmic inputs were immediately discarded. Recorded neurons had an average resting potential of –48 ± 1.3 mV, input resistance values of 189 ± 40 MΩ and series resistance averaged 19.1 ± 1.5 MΩ. Short voltage pulses (100 Hz, -10 mV, 3.0 ms) were used to estimate series resistance and whole-cell capacitance. The experiments where series resistance increased over 20% between control and trial conditions were excluded. Input resistance was calculated from the inverse of the slope of a linear regression line fitted to the I/V curves generated by depolarizing ramps from -90 to -40 mV.

Drugs and their application

In vivo. DL-Homocysteic acid (DLH)(1-10 mM) and Gallamine triethoiodide were obtained from Sigma-Aldrich (St. Louis, MO), while MRS 2365 (1 mM), adenosine (500 μM) and MRS 2279 (500 μM) were obtained from Tocris Biosciences (Bristol, UK). Pancuronium bromide was obtained from Alamone Labs (Jerusalem, Israel). Drugs were made up in HEPES-buffer (containing in mM; 137 NaCl, 5.4 KCl, 0.25 Na_2HPO_4, 0.44 KH_2PO_4, 1.3 $CaCl_2 \bullet 2H_2O$, 1.0 $MgSO_4 \bullet 7H_2O$, 4.2 $NaHCO_3$, 10 HEPES) to maintain neutral pH.

For preBötzinger drug injections, the head was tilted in the stereotaxic frame such that Bregma was 5 mm below Lambda (Gray *et al.*, 2001). Drugs or vehicle (HEPES-buffer) were pressure injected (Picospritzer III, Parker, Pine Brook, NJ) into the preBötC through a reticuled, sharp glass pipette (40 μm tip). The preBötC was located using stereotaxic coordinates (in mm) that, relative to obex, were 0.9 rostral, 2.0 lateral and 2.8 ventral. Injection volume was monitored by observing the movement of the meniscus relative to the reticule. An excitatory response to DLH (1-10 mM) confirmed positive location of the preBötC (Monnier *et al.*, 2003). MRS 2279 solution contained fluorescent microspheres (0.1 μm, yellow-green, 2% solids, Life Technologies) for histological identification of injection sites in relation to NK1 receptor immunolabeling.

In vitro. Adenosine triphosphate (ATP, 10 μM), MRS 2365 (10 μM, 100 μM), MRS 2279 (500 μM), DL-2-Amino-5-phosphono-pentanoic acid (AP5, 100 μM), thapsigargin (100 μM, 200 μM), cyclopiazonic acid (CPA, 100 μM) and SP ([Sar^9-$Met(O_2)^{11}$]-substance P (1 μM) were obtained from Tocris Biosciences. CNQX disodium salt (CNQX, 10 μM) and (+)-MK-801hydrogen maleate (MK-801, 100 μM) were obtained from Sigma-Aldrich (St. Louis, MO). Tetrodotoxin citrate (TTX, 0.5 μM) was purchased from Almone Labs (Jerusalem, Israel). Drugs were prepared as stock solutions in aCSF and frozen in aliquots except PPADS, suramin, TTX, CNQX, AP5 and MK-801 which were prepared in MilliQ (EMD Millipore, Billerica, MA) water. Thapsigargin and CPA required DMSO (0.2%) for

complete solubility. For drugs added in vitro, the final concentration of K^+ in the drug solution was matched to that of the aCSF.

Drugs were injected unilaterally into the preBötC via triple-barrelled pipettes (5-6 μm per barrel outer diameter). Drug microinjections were controlled by a programmable stimulator (Master-8; A.M.P.I., Jerusalem, Israel) connected to a picospritzer (~18 psi Spritzer4 Pressure Micro-Injector, Bioscience Tools, San Diego, CA). Consecutive agonist (MRS 2365) applications were separated by a minimum of 15 min. The suction electrode on the surface of the slice was used to guide the initial placement of the pipette. Substance P (1 μM) was then locally applied to functionally identify the preBötC based on a characteristic immediate, 3-4 fold increase in inspiratory frequency (Lorier *et al.*, 2007; Zwicker *et al.*, 2011). The injection site was moved in a grid-like fashion until the characteristic response was observed. When drugs (TTX, CNQX, AP5)were added directly to the circulating aCSF, they were given at least 10 min to equilibrate. During fluorescent imaging of inspiratory neurons, thapsigargin/CPA was given 30 minutes to equilibrate with the slice in a re-circulated bath (5ml/min, bath volume; 20 ml).

Data Analysis

Airflow, and electromyographic activity from the genioglossus and diaphragm muscles (GG_{EMG} and DIA_{EMG}) were acquired from spontaneously breathing rats. Airflow was measured via a pneumotach (GM instruments, Killwinning, Scotland UK) connected to a pressure transducer (Validyne, Northridge, CA) attached to the tracheal cannula and this signal was used to obtain frequency, tidal volume (V_T) and minute ventilation ($\dot{V}_E$). Parameters during drug application were compared with the average value during a two-minute control period preceding drug application. Peak drug effect was defined as the maximum value measured in a moving average of three consecutive bursts during the first minute after the injection.

Phrenic nerve activity, blood pressure and arterial blood gases were measured in paralyzed animals. Frequency, integrated phrenic nerve amplitude (∫PNA) and ventilatory output (frequency × ∫PNA) were calculated from the phrenic nerve recording in LabChart

(AD Instruments, Sydney, Australia), and exported to Microsoft Excel (Microsoft, Redmond, WA) for analysis. Respiratory parameters were calculated from 30-second time bins and reported relative to a two-minute control period preceding drug application. The HVR was characterized by comparing the peak values obtained during the initial hypoxia-induced increases in ventilation (phase I) and during the secondary depression when ventilation had plateaued (phase II). The peak value during phase I represents the group average of individual peak values obtained from a moving average measured during the first 1.5 min of hypoxia. Phase II values represent the average measured over the last 2 min of hypoxic exposure (shaded areas in Figs. 1, 6 and 7). All signals from the in vivo experiments were acquired and integrated in LabChart (AD Instruments, Sydney, Australia).

XII nerve activity from rhythmic slices was analyzed offline using Clampfit 9.2 software (Molecular devices, Sunnyvale, CA) and Microsoft Excel (Microsoft, Redmond WA). To assess the effects of a specific agent on the frequency response evoked by local injection of P2 receptor agonists into the preBötC, we compared the relative increase in peak frequency evoked by the agonist in control and in the presence of drug. Baseline frequency was the average frequency measured over the 2 min immediately prior to drug application. Peak frequency was the peak value in the first min of drug application obtained from a moving average calculated based on three consecutive XII bursts (Huxtable *et al.*, 2010; Zwicker *et al.*, 2011).

Differences between means were compared using either GraphPad Prism (Version 4, GraphPad Software Inc, La Jolla, CA) or SPSS (Version 20, IBM, North Castle, NY). For comparison of two groups, paired or unpaired t-tests were used as appropriate. For comparison of more than two groups, ANOVA was used in conjunction with either a Tukey or Bonferroni *post hoc* multiple comparison test. P values < 0.05 were considered significant. Group data are presented as boxplots created by the web-application 'BoxPlotR' (Spitzer *et al.*, 2014). Each boxplot details the spread of data points, which are superimposed on each box. Whiskers are defined by the lowest point, 1st quartile, median, 3rd quartile and highest point, denoted by the lower whisker, bottom, middle, top of box, and top whisker respectively. The mean for each group is denoted by "+".

RESULTS

Astroglial vesicular mechanisms contribute to the hypoxic ventilatory response in vivo

The expression of tetanus toxin light chain protein (TeLC) in astrocytes of the ventrolateral medulla (including, but not limited to the preBötC) to block vesicular release mechanisms attenuates the hypoxia-induced increase in ventilation in conscious adult rats (Angelova *et al.*, 2015). This reduced ventilatory response indicates a significant contribution of medullary astroglia to the hypoxia-induced increase in ventilation, by the release of gliotransmitters, namely ATP (Fig. 1 (ii)). The HVR, however, is biphasic, comprising of an initial increase (phase I) and a secondary depression to a lower steady-state (phase II). Thus, our first objective was to re-examine the contribution of glial vesicular release mechanisms to the HVR, specifically focusing on phases I and II of the HVR.

Five to seven days after viral injection, the rats were anesthetized, paralyzed, vagotomized and mechanically ventilated. Phrenic nerve activity, BP and blood gases were monitored and the HVR compared between three groups of rats: naïve, control animals expressing eGFP in medullary astrocytes, and rats expressing TeLC and eGFP in medullary astrocytes. Baseline parameters were measured in normoxia (30% O_2/70% N_2) for two min. Animals were then exposed to 5.5 min of hypoxia (10% O_2, 90% N_2) and returned to normoxia for two min. Sample traces from individual control and TeLC animals as well as time courses calculated for group data are shown in Fig. 2A, B and reported relative to baseline. Comparisons of phase I and II parameters for the three groups are reported in Fig. 2C. During phase I, the frequency and amplitude of the phrenic nerve discharge in naïve animals (n = 10) increased to a maximum of 1.41 ± 0.10 and 1.30 ± 0.04 of baseline respectively, giving a ventilatory output that was 1.79 ± 0.13 fold greater than the baseline. Rats transduced to express eGFP (n = 6) showed similar phase I increases in frequency, amplitude and the overall ventilatory output of 1.35 ± 0.04, 1.44 ± 0.09 and 1.83 ± 0.09, respectively. The phase I response of rats expressing TeLC in medullary astrocytes was

significantly reduced. Frequency and PNA amplitude were 1.16 ± 0.03 (n = 6) and 1.25 ± 0.04 (n = 6) of control. Ventilatory output increased to 1.35 ± 0.06 (n = 6) of baseline, which was significantly smaller than in the naïve rats and animals transduced to express eGFP ($p = 0.038$, $p = 0.041$ One-way ANOVA, Tukey post-hoc test).

During phase II of the HVR, the increases in frequency and PNA amplitude were not significantly different between the three groups. Frequency was 1.16 ± 0.07, 1.15 ± 0.04 and 0.97 ± 0.04, and PNA amplitude was 1.28 ± 0.04, 1.29 ± 0.08 and 1.17 ± 0.04 for naïve, viral control and TeLC expressing rats, respectively. Ventilatory output, however, was significantly lower in the TeLC expressing rats (1.12 ± 0.04) compared to naïve (1.49 ± 0.09) and eGFP expressing rats (1.48 ± 0.09) ($p = 0.024$, 0.048, One-way ANOVA, Tukey post-hoc test). These data indicate that the vesicular release of gliotransmitters by preBötC astrocytes contributes to the enhanced ventilatory activity in both phases of the HVR.

Postmortem analysis of serial 50 μm transverse brainstem sections from animals expressing eGFP and TeLC in medullary astrocytes revealed the extent of viral expression across the ventral respiratory column (VRC) (Fig. 3A). Viral expression was similar in both groups. It was strongest at the level of the preBötC where the injection pipette tracts were visible. The injection sites were located ~750-850 μm caudal to the caudal border of the facial nucleus at the same level as anatomical markers of the preBötC (lateral loop of the principal subnucleus of the inferior olive and the semi-compact division of nucleus ambiguus, just caudal to its compact formation (Paxinos & Watson, 2007; Ruangkittisakul *et al.*, 2008). The strongest viral expression also overlapped with the site along the VRC with the highest density of NK1 receptor immunolabeling (Fig. 3B), an established marker of the preBötC (Gray *et al.*, 1999; Guyenet & Wang, 2001; Guyenet *et al.*, 2002). Viral expression dropped off substantially 500 μm rostral and caudal to the injection site centered in the preBötC (Fig. 3A).

The morphology of all eGFP and TeLC-expressing cells was consistent with astrocytic targeting, as described in detail previously (Gourine *et al.*, 2010; Angelova *et al.*, 2015). The selectivity of our viral vectors in transfecting medullary astrocytes has been demonstrated (Liu *et al.*, 2008; Gourine *et al.*, 2010; Tang *et al.*, 2014). To further ensure

the specificity, we examined 253 transduced cells from 3 sections from 3 different animals for co-localization of eGFP expression with the immunoreactivity for a neuron specific marker, NeuN. A representative example of eGFP and NeuN immunostaining and their overlay is shown in Fig. 3C. Ten NeuN labeled cells are circled to facilitate comparison. None of the NeuN labeled cells were transduced to express eGFP.

$P2Y_1$ receptor activation in the preBötC increases respiratory frequency in adult rats in vivo

The experiments involving blockade of astroglial vesicular mechanisms using TeLC described above do not identify the gliotransmitter(s) that excites the preBötC network, but substantial evidence points to the involvement of ATP (Gourine *et al.*, 2005; Angelova *et al.*, 2015). The next objective was to assess whether $P2Y_1$ receptors mediate the actions of ATP in the preBötC in vivo (Fig. 1, (iii)). Local injection of ATP into the preBötC of neonatal rhythmically-active medullary slices causes a site-specific, $P2Y_1$ receptor-mediated increase in inspiratory-related frequency (Lorier *et al.*, 2004; Lorier *et al.*, 2007). We therefore tested whether local, unilateral injection of the $P2Y_1$ receptor agonist, MRS 2365 (1 mM, n = 8) into the preBötC of anesthetized, vagotomized spontaneously-breathing adult rats increases respiratory frequency.

The preBötC was functionally identified based on the stereotypical response to a microinjection of DLH (10 mM) that comprises a rapid-onset increase in inspiratory frequency and decrease in burst amplitude (Monnier *et al.*, 2003), as shown in Fig. 4A. If a response was not evoked at the initial site the pipette was moved in a grid-like manner until the expected response was observed. The excitatory effect of DLH was limited to a relatively small area. Injections 200 µm rostral to the preBötC (presumably in the BötC) reduced inspiratory frequency (Fig. 4B) while injections 300 µm caudal had no effect on breathing (Fig. 4C).

A typical response of MRS2365 injection into the preBötC is illustrated in Fig. 5A. This recording, its corresponding time course (Fig. 5B) and group data (Fig. 5C) show that MRS 2365 microinjections into the preBötC in vivo significantly increased respiratory

frequency to 1.44 ± 0.09 of control (p = 0.0013). V_T decreased to 0.60 ± 0.09 of control (p = 0.0054). The amplitude of ∫DIAEMG and ∫GGEMG (not shown) inspiratory bursts decreased similarly to 0.60 ± 0.10 (p = 0.0049) and 0.60 ± 0.05 (p = 0.0002) of control, respectively (Fig. 5C). The increase in frequency and decrease in V_T offset each other such that minute ventilation (V_E) was not significantly affected by $P2Y_1$ receptor activation, as expected in an actively breathing animal with intact chemoreceptor feedback mechanisms. Control (saline) injections into the same brainstem sites had no significant effect on the respiratory frequency, V_T or V_E.

Histological analysis of brainstem sections confirmed the functional DLH mapping. The fluorescent microspheres that marked the MRS 2365 injection sites were localized in a region corresponding to the preBötC based on anatomical criteria and the relationship to NK1 receptor immunolabeling as described above (Fig. 5D). Injection sites are mapped onto a schematic (Fig. 5D, left side). A representative injection site (red fluorescence) is also shown (Fig. 5D, right side).

Adenosine injection into the preBötC has no effect on ventilation in adult rats in vivo

Extracellular ATP is degraded rapidly by ectonucleotidases ultimately into adenosine, which can inhibit respiratory activity (Herlenius *et al.*, 1997; Huxtable *et al.*, 2009; Zwicker *et al.*, 2011). However, sites, mechanisms and the effects of adenosine appear to be species- and age-dependent (Huxtable *et al.*, 2009; Zwicker *et al.*, 2011). In the rat in vitro, adenosine application in the preBötC inhibits inspiratory frequency from embryonic stages until P2-3 (Herlenius *et al.*, 1997; Huxtable *et al.*, 2009). To determine whether the generation of adenosine from hydrolyzed ATP could could have a confounding influence on responses evoked by ATP released by preBötC astrocytes in adult rats, we microinjected adenosine (500 nl, 500 μM) unilaterally into the preBötC of adult, anesthetized, vagotomized rats. The representative traces and group data (Fig. 6A and C) show that injections of adenosine had no significant effect on ventilation. Frequency, V_T and V_E were 1.09 ± 0.03, 1.02 ± 0.01 and 1.09 ± 0.02 of control, respectively (n = 7, paired t-test p > 0.05). Responses elicited by DLH delivery into the same brainstem sites

confirmed that the injections were placed within the preBötC (Fig. 6C). DLH caused a significant and rapid 1.36 ± 0.05 fold ($p = 0.004$) increase in frequency and parallel decrease in V_T to 0.67 ± 0.04 of control ($p = 0.002$) (Fig. 6C). Fluorescently-marked adenosine injection sites mapped to the preBötC based on anatomical landmarks (Fig. 6D). Fig. 6E shows a high magnification fluorescent image in which fluorescent microspheres that mark the injection site are in a region of strong NK1 receptor immunoreactivity.

$P2Y_1$ receptor blockade in the preBötC of adult rats increases the secondary hypoxic respiratory depression

Given that ATP released in the ventral respiratory column during hypoxia counteracts the secondary respiratory depression (Gourine *et al.*, 2005), and that ATP evokes $P2Y_1$ receptor mediated increases in respiratory activity by acting within the preBötC in vitro (Lorier *et al.*, 2007) and in vivo (Fig. 5), we tested the hypothesis that the secondary hypoxic depression is counteracted by ATP-induced activation of $P2Y_1$ receptors in the preBötC (Fig. 1 (iii)). We compared the HVRs of adult, urethane-anesthetized, paralyzed, mechanically ventilated and vagotomized rats following unilateral microinjections of vehicle (0.2 µl HEPES buffer) or the $P2Y_1$ receptor antagonist, MRS 2279 (0.2 µl, 500 µM) into the preBötC, two min prior to the onset of hypoxia. Integrated phrenic nerve activity (∫PNA) was monitored as an index of central respiratory drive for two min in normoxia (30% O_2 - 70% N_2), five min in hypoxia (10% O_2 - 90% N_2) and then during the return to normoxia. Vehicle and MRS 2279 hypoxia trials were separated by one hour to ensure that the animals had fully recovered from the first hypoxic challenge. Representative recordings of ∫PNA in Fig. 7 show the hypoxic responses of one animal after vehicle and MRS 2279 microinjections into the preBötC. Blockade of $P2Y_1$ receptors with MRS 2279 had no effect on the initial phase I of the HVR. In the control (after microinjections of the vehicle) hypoxia trials, frequency, burst amplitude and ventilatory output increased in phase I to levels that were 1.42 ± 0.08, 1.52 ± 0.11, and 1.83 ± 0.23 fold greater than baseline, respectively. In MRS 2279, hypoxia evoked phase I increases in frequency, burst amplitude and ventilatory output that were 1.17±0.06, 1.23 ± 0.06 and

1.36±0.11 of baseline. Only the change in burst amplitude was significantly reduced compared to control during phase I (p=0.038, paired t-test, n=6).

In contrast, MRS 2279 significantly reduced the respiratory activity during phase II of the HVR. In the vehicle trials, during phase II, frequency fell to 0.95 ± 0.07 of baseline and burst amplitude remained elevated at 1.34 ± 0.09 of baseline such that ventilatory output remained above the baseline level recorded during normoxia (1.28 ± 0.15). After MRS 2279 application, frequency and V_E fell to the levels significantly below that seen in the vehicle controls and below baseline. Frequency fell to 0.62 ± 0.10 (p = 0.045, paired t-test, n = 6) of control while ventilatory output was 0.73 ± 0.14 (p = 0.0270, paired t-test, n = 6) of baseline. Group data are summarized in Fig. 7B Injection sites marked with fluorescent microspheres localized to the preBötC anatomically and based on the pattern of NK1 receptor immunolabeling (Fig. 7C).

To ensure that the greater hypoxic depression following MRS 2279 microinjections into the preBötC was not due to time-dependent changes in the HVR with repeated hypoxic exposures, we performed a control series of experiments in which the hypoxia protocol was repeated at a one hour interval but the first and second hypoxic challenges were preceded by a vehicle injection. The frequency, ∫PNA amplitude and ventilatory output responses to the two consecutive hypoxic responses were not significantly different (Fig. 8, n=5). Comparison of the second hypoxia response in this time control series with the hypoxia response in MRS 2279 from the previous series (i.e., unpaired data) also showed that during phase II MRS 2279 caused a significant reduction in both frequency and ventilatory output (p = 0.01 and 0.03 respectively, independent samples t-test).

Increases in $[Ca^{2+}]_i$ contribute to the excitatory actions of $P2Y_1$ receptor activation on the inspiratory rhythm generated by the preBötC

Activation of $P2Y_1$ receptors in the preBotC increases respiratory activity in vivo and in vitro (Funk *et al.*, 1997; Lorier *et al.*, 2004; Lorier *et al.*, 2007; Lorier *et al.*, 2008; Huxtable *et al.*, 2009; Zwicker *et al.*, 2011). We used rhythmic slice preparations to examine the signaling pathways via which $P2Y_1$ receptor activation excites the preBötC

network. Analyses of recombinant $P2Y_1$ receptors and native $P2Y_1$ receptors in other brain regions indicate that responses depend on increases in $[Ca^{2+}]_i$ (Rajani *et al.*, 2015). As depicted in Fig. 1, $[Ca^{2+}]_i$ dependent pathways can increase excitability by modulating the activity of multiple ion channels (Fig. 1 iv, v). We therefore tested the hypothesis that increases in $[Ca^{2+}]_i$ are necessary for $P2Y_1$ receptor activation to increase inspiratory frequency. We compared the responses of the preBötC network to local MRS 2365 administered after local application of vehicle or the Ca^{2+} chelator, EGTA-AM (1 mM). We used MRS 2365 rather than ATP because the frequency effect is mediated by $P2Y_1$ receptors and because MRS 2365 avoids the confounding inhibitory actions on neonatal networks of adenosine that is generated from the degradation of ATP by endogenous ectonucleotidases. Vehicle and EGTA-AM (1 mM) were locally applied to the preBötC for 5 min (5 s on, 5 s off), prior to local application of MRS 2365 (10 s, 100 μM). As shown for a single slice preparation and group data in Fig. 9A, EGTA-AM significantly reduced the MRS 2365 response from a 2.1 ± 0.14 fold increase in control to a 1.5 ± 0.08 fold increase in EGTA-AM (n = 6, p = 0.0047, paired t-test).

To assess whether the increase in intracellular Ca^{2+} that contributes to the $P2Y_1$ receptor evoked frequency increase is derived from intracellular sources, we next compared control MRS 2365 responses evoked after vehicle application with those evoked after local application of thapsigargin (200 μM) to the preBötC, a sarco/endoplasmic reticulum Ca^{2+} ATPase (SERCA) inhibitor that depletes intracellular calcium stores. The target of thapsigargin is intracellular. Thus, additional time was allowed for thapsigargin to diffuse into the tissue and cross cell membranes. MRS 2365 applications were preceded by 30 minutes of pre-application (5s on, 5s off) of vehicle or thapsigargin. The response of a single preparation and group data are shown in Fig. 9C and 9D, respectively. Following 30 minutes of application, thapsigargin reduced the MRS 2365 evoked frequency increase from a 2.59 ± 0.15 fold increase to 1.90 ± 0.21 (n = 6, p=0.007, paired t-test). A series of control experiments comparing the response of MRS 2365 before and after 30 min local application of DMSO (0.2%) established that the thapsigargin-mediated inhibition was not due to the actions of the vehicle. Vehicle application for 30 minutes did not affect the MRS 2365 response (n=5, p>0.05, paired t-test).

$P2Y_1$ receptor activation increases Ca^{2+}_i in preBötC inspiratory neurons and glia

The EGTA and thapsigargin induced reductions in the $P2Y_1$ receptor-evoked frequency increase indicates that increases in $[Ca^{2+}]_i$ are an important part of ATP mediated excitatory signaling in the preBötC. These data, however, do not establish whether the ATP-evoked frequency increase depends on an increase in neuronal $[Ca^{2+}]_i$, (Fig. 1 iv), glial $[Ca^{2+}]_i$, (Fig. 1 ii) or both. To gain insight into the cells that mediate the network excitation we tested whether inspiratory neurons and glia in the preBötC respond to ATP with an increase in $[Ca^{2+}]_i$.

To test neuronal sensitivity we loaded the preBötC of rhythmic slices with the Ca^{2+}-sensitive dye, Fluo-4. Fluo-4 fluorescence and XII inspiratory nerve activity were recorded during local application of MRS 2365 (100 μM) to the preBötC. Inspiratory neurons were identified by rhythmic increases in the Fluo-4 signal in phase with the rhythm recorded from the XII nerve (Fig. 10). Five such neurons are marked with arrows in Fig. 10A and their baseline, inspiratory-related oscillations in $[Ca^{2+}]_i$ are apparent in the recordings of fluorescence intensity (Fig. 10B). Local application of MRS 2365 (100 μM) near the surface of the slice evoked significant increases in preBötC frequency and the Fluo-4 signal in all 5 inspiratory neurons imaged in this slice (Fig. 10B). Group data taken from 18 inspiratory neurons in 5 slices showed a similar 1.53 ± 0.06 fold increase in the fluo-4 $[Ca^{2+}]_i$ signal (Fig. 10C) (n=18 from 5 slices, $p < 0.0001$, paired t-test).

To test whether the MRS 2365-evoked increase in $[Ca^{2+}]_i$ derives from intracellular sources, we compared the MRS 2365 response in control (1 min, 10 μM) with that evoked after the SERCA blocker thapsigargin (100 μM) or CPA (100 μM) was bath applied for 30 minutes. To account for any changes to the MRS 2365-evoked fluorescence due to photobleaching, two consecutive control MRS 2365 applications were applied 30 minutes apart. The second control MRS 2365 response was then followed by the application of thapsigargin or CPA for 30 min and another MRS 2365 application. Two inspiratory neurons are marked in Fig 10D, along with their Fluo-4 fluorescence signals in Fig 10E. We compared the decrease in fluorescence that occurred between MRS 2365 control trial 1

and control trial 2 with the decrease observed between control trial 2 and the trial with SERCA blockers. Thapsigargin (n=8 neurons, 4 slices) and CPA (n=4 neurons, 1 slice) had similar effects on the MRS 2365 evoked increase in Ca^{2+} fluorescence, so these data were pooled (n=12 neurons, 5 slices). There was only a small decrease in Ca^{2+} fluorescence between the two control trials; trial 2 response was 95.0 ± 2.7 % of the first. In marked contrast, the reduction in the Ca^{2+} fluorescence response between the MRS 2365/thapsigargin trial and control trial 2 was significantly greater than the reduction in the MRS 2365 fluorescence response that occurred between control trials 1 and 2. In thapsigargin/CPA, the MRS 2365 evoked fluorescence increase was only 43.9 ± 7.3% of control trial 2 (n=12, $p<0.0001$, paired t-test) (Fig. 10F).

While the preBötC is the critical site for inspiratory rhythm generation, it contains multiple subtypes of inspiratory-related neurons that can be differentiated based on embryonic origin (Dbx1), peptide (SST) or peptide receptor (NK1, μ-opioid) expression, presence or absence of pacemaker properties and whether they are excitatory (glutamatergic) or inhibitory (GABAergic). The high sensitivity of the preBötC network to $P2Y_1$ receptor excitation suggests that there may be a specific excitatory, ATP-sensitive population of preBötC neurons that either generates rhythm or provides drive to rhythm generating neurons. In contrast, if diverse excitatory and inhibitory preBotC inspiratory neurons are ubiquitously excited by ATP, one might predict blunted network sensitivity to ATP. As an initial foray into this important question, we simply asked whether all inspiratory modulated preBötC neurons are sensitive to $P2Y_1$ receptor activation. As above, we used Ca^{2+}-imaging of Fluo4-loaded rhythmic slices, identified inspiratory neurons based on rhythmic Ca^{2+} oscillations in phase with XII nerve output and counted cells that did or did not respond to MRS 2365 with an increase in Ca^{2+} fluorescence. In these experiments, MRS 2365 was bath-applied to activate as many neurons as possible and to prevent false negatives that can occur with local application when the drug does not diffuse from the pipette to the neuron in question. Neurons were only counted as weak- or nonresponders if there were other neurons in the same field of view that showed a strong response to MRS 2365. When all the data were grouped, 20 neurons from 7 slices showed an average 30.8+6.8% increase in fluorescence above baseline (data not shown). However, these 20

neurons could be divided into weak/non-responders and responders. Eight of the 20 neurons responded to MRS 2365 with an average increase in fluorescence of only 6.5+2.8%. The remaining 12 neurons were on average 7 times more sensitive, responding with a average 46.9+10.4% increase in fluorescence.

To explore the signaling pathways through which ATP excites preBötC glial cells, glia were isolated from preBötC tissue punches and grown in culture using sorbitol in place of glucose as the metabolic substrate since only glia can utilize sorbitol. Cultures were loaded with Fluo-4-AM. Local application of ATP (10 μM, 10 s) evoked a 3.08 ± 0.2-fold increase in Ca^{2+} related fluorescence (Fig. 11), which we have shown previously is primarily mediated by $P2Y_1$ receptors (i.e., it is blocked by MRS 2279 but neither suramin nor PPADS (Huxtable *et al.*, 2010). Images of baseline fluorescence, the peak ATP response in control and after bath application of the SERCA blocker, thapsigargin (50 nM, 30 min), are shown for a group of cultured glial cells in Fig. 11A, along with the time course of fluorescence changes for four of these cells in Fig. 11B. Bath application of thapsigargin virtually blocked the ATP-evoked increase in Ca^{2+} related fluorescence which rose to only 1.18 ± 0.03 of baseline (Fig. 11B, n = 53 cells, $p<0.001$, paired t-test).

ATP-induced excitation of preBötC neurons does not involve glia-derived glutamate

PreBötC astrocytes respond to hypoxia with an increase in $Ca^{2+}{}_i$ and exocytotic release of ATP (Angelova, et al 2015). They also respond to ATP (Fig. 11; (Huxtable *et al.*, 2010), raising the possibility that during hypoxia, the autocrine/paracrine activation of astrocytes by ATP evokes additional gliotransmitter release that contributes to the HVR (Fig 1. vi). ATP and glutamate are major gliotransmitters that are released from cultured preBotC glia in response to hypoxia (Angelova et al., 2015) or ATP, respectively (Huxtable et al 2010). We asked whether activation of astrocytes by ATP can evoke the release of gliotransmitters that, in turn, affect the excitability of inspiratory neurons. We tested this indirectly by determining whether stimulation of astrocytes with exogenous ATP evokes glutamate-mediated excitation of inspiratory neurons. In rhythmic slices, we obtained whole-cell voltage clamp recordings from preBötC inspiratory neurons, identified by

rhythmic synaptic inputs in phase with inspiratory-related bursts in the XII nerve. We then applied TTX (0.5 μM) to block action potential dependent transmitter release and compared the neuronal response to locally applied ATP before and during application of glutamate receptor antagonists, CNQX (10 μM) and AP5 (100 μM)/MK-801 (100 μM) (n=8). CNQX/AP5 was used in 3 of 8 experiments while CNQX/MK-801 was used in the other 5. Data were pooled since effects of AP5 and MK801 were the same. Because locally applied ATP can stimulate astrocytes and neurons, we predicted that if glial-derived glutamate contributes to the neuronal ATP response, the ATP current would decrease in CNQX and AP5/MK-801. Due to the potential for time-dependent reduction in the amplitude of ATP currents, data obtained in the CNQX and AP5/MK-801 protocol were compared with a time-matched control group that received repeated ATP injections at 15 min intervals. ATP currents are reported as a ratio of the difference between the ATP current amplitudes evoked in the first and second applications divided by the first current. A value of zero indicates that the first and second ATP currents were the same, a negative value indicates the second response was smaller than the first and vice versa. Fig. 12A shows a representative voltage clamp recording from an inspiratory neuron and currents evoked by ATP in control (pre-TTX, rhythmic inspiratory synaptic currents are present), after TTX and again after application of CNQX and AP5. The current traces and group data both indicate that there is no effect of glutamate receptor antagonism on the ATP current. The ATP current evoked in TTX plus CNQX+AP5/MK-801 groups was 0.2 ± 8.0% smaller than the first. In the time-control group, ATP responses decreased 6.4 ± 4.7% between first and second applications. We did not examine ATP-evoked ATP release from astrocytes because P2 receptor antagonists would block the initial ATP response.

DISCUSSION

The biphasic ventilatory response of mammals to acute, moderate hypoxia comprises an initial, phase I increase in the first minute that is attributed to peripheral chemoreceptors, followed by a centrally-mediated secondary depression over several minutes to a new steady state phase II level. Our data complement emerging evidence of a

central component to the excitation where glia act as hypoxia sensors and release ATP, exciting the respiratory network and offsetting the secondary respiratory depression (Angelova *et al.*, 2015). We advance mechanistic understanding by showing that the actions of ATP in the HVR are mediated in the preBötC through activation of $P2Y_1$ receptors that increase inspiratory frequency in vitro via thapsigargin-sensitive increases in $[Ca^{2+}]_i$ that occur in both inspiratory neurons and astroglia.

The role of glia and ATP in phase I and phase II of the hypoxic ventilatory response

Evidence for gliotransmission in the intact CNS is sparse, reflecting the difficulty of selectively manipulating glial function. The contribution of gliotransmission to the HVR was first demonstrated by the reduction of the HVR in freely-moving rats following blockade of glial exocytosis through bilateral expression of TeLC in preBötC/VRC astrocytes (Angelova *et al.*, 2015). Here, in paralyzed, mechanically ventilated rats, blockade of vesicular transmitter release in glia using TeLC suggests that gliotransmission contributes to both phases of the HVR.

Unilateral microinjection of MRS 2279 into the preBötC, in contrast, did not affect the phase I increase, indicating that $P2Y_1$ receptors in the preBötC do not contribute. Two protocol differences might account for this discrepancy. First, since TeLC blocks all vesicular release mechanisms but MRS 2279 selectively antagonizes $P2Y_1$ receptors, the reduction of ventilation in phase I by TeLC may indicate a contribution of a non-$P2Y_1$ receptor-mediated component. Astrocytes release multiple transmitters, including glutamate and D-serine, that could stimulate ventilation. ATP evokes glutamate release from cultured preBötC glia (Huxtable *et al.*, 2010), but stimulation of glia in rhythmic slices with ATP does not cause glutamatergic excitation of inspiratory neurons (Fig. 12).

Second, the region of the brainstem affected was different between TeLC and MRS 2279 protocols. TeLC injections were bilateral and centered in the preBötC, but expression extended up to >500 μm rostrally and caudally from the center of the injection site in preBötC. The MRS 2279 injections were unilateral and, if MRS 2279 and DLH have similar diffusion profiles, likely extended less than 200 μm. Given that the bulk of evidence

supports that the phase I response is mediated by carotid body chemoreceptors (Bureau *et al.*, 1985; Fung *et al.*, 1996; Prabhakar, 2000), the physiological significance of the TeLC-mediated inhibition of the phase I response must be interpreted cautiously until the underlying mechanism is established.

Our conclusion that gliotransmission contributes to the HVR depends on the selectivity of the bidirectional sGFAP-based vector system to interfere with exocytosis only in astrocytes. Glial specificity of this vector system (Liu *et al.*, 2008; Gourine *et al.*, 2010; Tang *et al.*, 2014), and efficacy of TeLC in blocking exocytosis have been established (Angelova *et al.*, 2015). Our analysis of transfected brain sections further suggests that TeLC expression is specific to astrocytes when under the control of the sGFAP promoter; no cells were detected that expressed eGFP and displayed NeuN immunoreactivity.

ATP acts via $P2Y_1$ receptors to increase ventilation in vivo

P2 receptors comprise seven ionotropic P2X (North, 2002) and eight metabotropic P2Y (Abbracchio *et al.*, 2003) subtypes. $P2Y_1$ receptor immunolabeling is prevalent throughout the VLM (Fong *et al.*, 2002) and overlaps with intense NK1 receptor expression, an established marker of the preBötC. Indeed, $P2Y_1$ receptors underlie the excitatory actions of ATP in the preBötC in vitro (Lorier *et al.*, 2007). Here we translate these in vitro findings and reveal, using unilateral injections of MRS 2279, that endogenous activation of preBötC $P2Y_1$ receptors in vivo increases ventilation and attenuates the secondary hypoxic respiratory depression. The fact that antagonists were only applied unilaterally means that our measurements may underestimate the magnitude of the $P2Y_1$ receptor-mediated increases in ventilation during hypoxia. Whether $P2Y_1$ receptors are the only P2 receptor subtype involved in the HVR is uncertain, as a variety of P2 receptors are expressed in the VRC (Thomas *et al.*, 2001; Fong *et al.*, 2002; Gourine *et al.*, 2003; Lorier *et al.*, 2004; Lorier *et al.*, 2007). Nonetheless, our data illustrate a significant role for $P2Y_1$R in the ATP-induced increase in ventilation in the preBötC during hypoxia.

Adenosine inhibition of the preBötC network does not contribute to the hypoxic respiratory depression in adult rat

Experiments were not designed to identify the mechanisms underlying the hypoxic respiratory depression, but our data provide some insight. First, the $P2Y_1$ receptor-mediated attenuation indicates that the secondary depression is not shaped by a single inhibitory mechanism. Second, adenosine inhibition of the preBötC network does not contribute to the depression in adult rats. The enhanced hypoxic respiratory depression observed in adults rats expressing the ectonucleotidase TMPAP in the preBötC and VRC (Angelova *et al.*, 2015) is due to degradation of excitatory ATP rather than accumulation of adenosine. Also, hypoxia-induced adenosine release has been detected in the NTS of adult rats, but not in the VLM (Gourine *et al.*, 2002).

Developmentally, adenosine plays a more important role. An A1 receptor inhibitory mechanism is implicated in the secondary hypoxic depression in a host of premature/newborn mammals including pigs, sheep, (Moss, 2000), rats and mice (Funk *et al.*, 2008; Huxtable *et al.*, 2009; Zwicker *et al.*, 2011). Developmental analyses are required in multiple species to assess whether A1 inhibitory mechanisms disappear postnatally, as occurs in P2-3 rats (Herlenius *et al.*, 1997; Huxtable *et al.*, 2009). Medullary and suprapontine A2a receptor-mediated excitation of GABAergic inhibitory neurons may also contribute to the depression in piglets and fetal sheep (Koos & Maeda, 2001; Koos *et al.*, 2001; Wilson *et al.*, 2004).

Signaling pathways of the $P2Y_1$ receptor-mediated excitation; neurons versus glia

The only identified source of extracellular ATP during hypoxia is from astrocytes (Angelova *et al.*, 2015). Thus, our working hypothesis is that, during hypoxia, astrocyte-derived ATP increases inspiratory frequency primarily through excitation of preBötC inspiratory neurons but also through autocrine/paracrine excitation of astrocytes causing further gliotransmitter release (Fig. 1 iii, vi). Consistent with this hypothesis, both preBötC inspiratory neurons (in slices, Fig. 10) and preBötC glia (in slices and culture (Fig. 11)

(Huxtable *et al.*, 2010)) respond to ATP via a $P2Y_1$ receptor signaling pathway that involves a thapsigargin-sensitive increase in $[Ca^{2+}]_i$ and a neuronal inward current (Lorier et al., 2008). The ion channels underlying this inward current have yet to be identified, though candidates have been proposed (Rajani *et al.*, 2015).

ATP-induced excitation of neurons is clearly involved in preBötC excitation. However, a role for autocrine/paracrine excitation of astrocytes by ATP remains to be established. Autocrine/paracrine excitation was first implicated with the observations that glial toxins attenuate the frequency increase evoked by ATP in the preBötC in vitro and that cultured preBötC astrocytes release glutamate in response to ATP (Huxtable *et al.*, 2010). In contrast, imaging of cultured brainstem astrocytes suggests that ATP does not signal via paracrine/autocrine mechanisms; low pH and hypoxia-evoked fusion of putative ATP-containing vesicles was unaffected by ATP degrading enzymes or $P2Y_1$ receptor antagonists (Kasymov *et al.*, 2013; Angelova *et al.*, 2015). The sparse nature of these astrocyte cultures could have compromised detection of autocrine/paracrine signaling. However, our whole-cell data showing that ATP does not evoke glutamatergic excitation of inspiratory neurons suggest that preBötC astrocytes in situ do not respond to ATP by releasing a transmitter, and that autocrine/paracrine ATP signaling may not contribute to the HVR.

$[Ca^{2+}]_i$ increases contribute to $P2Y_1$ receptor-mediated inspiratory frequency increase

Analysis of recombinant receptors suggests that $P2Y_1$ receptors predominantly signal through the $G\alpha_{q/11}$ pathway, which involves activation of PLC, release of Ca^{2+} from intracellular stores, and DAG-mediated activation of protein kinase C (Simon *et al.*, 1995; von Kugelgen & Wetter, 2000; Sak & Illes, 2005). Here we show that an increase in $[Ca^{2+}]_i$ contributes to the $P2Y_1$-mediated frequency increase in vitro, which implicates a $[Ca^{2+}]$-dependent, second messenger pathway that is dependent on $[Ca^{2+}]_i$. The ATP/MRS 2365-mediated frequency increase, however, was not completely blocked by EGTA-AM or thapsigargin (Fig. 9). Thus, either the block of $[Ca^{2+}]_i$ changes was incomplete or Ca^{2+}-insensitive pathways may contribute. $P2Y_1$ receptors can also signal through $G\alpha_i$ and alter

ion channel activity through the membrane-delimited βγ subunit without changing $[Ca^{2+}]_i$ (Brown *et al.*, 2000; Filippov *et al.*, 2000; Aoki *et al.*, 2004). To fully elucidate these mechanisms, a deeper exploration of signalling pathways and downstream candidate ion channels underlying the $P2Y_1$-evoked excitation of the preBötC is required (Rajani *et al.*, 2015).

Significance

Understanding the multitude of factors that determine the dynamics of the HVR is key in the development of strategies to counteract the hypoxia-induced depression of breathing. We have identified an endogenous $P2Y_1$ receptor mechanism that attenuates this depression in adults and is active in embryonic stages through to adulthood in mammals. Degradation of ATP in the preBötC will contribute to the depression by removing excitatory actions of ATP, but also by producing adenosine, which is inhibitory in the perinatal period and variably into adulthood. Strategies to minimize the hypoxic depression of ventilation should aim to enhance $P2Y_1$ receptor-mediated signaling, inhibit ATP degradation and enhance removal of adenosine from the extracellular space.

REFERENCES:

Abbracchio MP, Boeynaems J-M, Barnard EA, Boyer JL, Kennedy C, Miras-Portugal MT, King BF, Gachet C, Jacobson KA, Weisman GA & Burnstock G. (2003). Characterization of the UDP-glucose receptor (re-named here the P2Y14 receptor) adds diversity to the P2Y receptor family. *Trends Pharmacol Sci* **24,** 52-55.

Angelova PR, Kasymov V, Christie I, Sheikhbahaei S, Turovsky E, Marina N, Korsak A, Zwicker J, Teschemacher AG, Ackland GL, Funk GD, Kasparov S, Abramov AY & Gourine AV. (2015). Functional Oxygen Sensitivity of Astrocytes. *J Neurosci* **35,** 10460-10473.

Aoki Y, Yamada E, Endoh T & Suzuki T. (2004). Multiple actions of extracellular ATP and adenosine on calcium currents mediated by various purinoceptors in neurons of nucleus tractus solitarius. *Neurosci Res* **50,** 245-255.

Brown DA, Filippov AK & Barnard EA. (2000). Inhibition of potassium and calcium currents in neurones by molecularly-defined P2Y receptors. *Journal of the Autonomic Nervous System* **81,** 31-36.

Bureau MA, Lamarche J, Foulon P & Dalle D. (1985). The ventilatory response to hypoxia in the newborn lamb after carotid body denervation. *Respir Physiol* **60,** 109-119.

Filippov AK, Brown DA & Barnard EA. (2000). The P2Y1 receptor closes the N-type Ca2+ channel in neurones, with both adenosine triphosphates and diphosphates as potent agonists. *Br J Pharmacol* **129,** 1063-1066.

Fong AY, Krstew EV, Barden J & Lawrence AJ. (2002). Immunoreactive localisation of P2Y1 receptors within the rat and human nodose ganglia and rat brainstem: comparison with [alpha 33P]deoxyadenosine 5'-triphosphate autoradiography. *Neuroscience* **113,** 809-823.

Fung ML, Wang W, Darnall RA & St John WM. (1996). Characterization of ventilatory responses to hypoxia in neonatal rats. *Respir Physiol* **103,** 57-66.

Funk G, Huxtable A & Lorier A. (2008). ATP in central respiratory control: A three-part signaling system. *Respiratory Physiology & Neurobiology* **164,** 131-142.

Funk GD. (2013). Neuromodulation: Purinergic Signaling in Respiratory Control. *Comprehensive Physiology* **3,** 331-363.

Funk GD, Kanjhan R, Walsh C, Lipski J, Comer AM, Parkis MA & Housley GD. (1997). P2 receptor excitation of rodent hypoglossal motoneuron activity in vitro and in vivo: a molecular physiological analysis. *J Neurosci* **17,** 6325-6337.

Gourine AV, Atkinson L, Deuchars J & Spyer KM. (2003). Purinergic signalling in the medullary mechanisms of respiratory control in the rat: respiratory neurones express the P2X2 receptor subunit. *J Physiol* **552,** 197-211.

Gourine AV, Kasymov V, Marina N, Tang F, Figueiredo MF, Lane S, Teschemacher AG, Spyer KM, Deisseroth K & Kasparov S. (2010). Astrocytes Control Breathing Through pH-Dependent Release of ATP. *Science* **329,** 571-575.

Gourine AV, Llaudet E, Dale N & Spyer KM. (2005). Release of ATP in the ventral medulla during hypoxia in rats: role in hypoxic ventilatory response. *Journal of Neuroscience* **25,** 1211-1218.

Gourine AV, Llaudet E, Thomas T, Dale N & Spyer KM. (2002). Adenosine release in nucleus tractus solitarii does not appear to mediate hypoxia-induced respiratory depression in rats. *J Physiol* **544,** 161-170.

Gray PA, Janczewski WA, Mellen N, McCrimmon DR & Feldman JL. (2001). Normal breathing requires preBötzinger complex neurokinin-1 receptor-expressing neurons. *Nat Neurosci* **4,** 927-930.

Gray PA, Rekling JC, Bocchiaro CM & Feldman JL. (1999). Modulation of respiratory frequency by peptidergic input to rhythmogenic neurons in the preBötzinger complex. *Science* **286,** 1566-1568.

Guyenet PG, Sevigny CP, Weston MC & Stornetta RL. (2002). Neurokinin-1 Receptor-Expressing Cells of the Ventral Respiratory Group Are Functionally Heterogeneous and Predominantly Glutamatergic. *The Journal of Neuroscience* **22,** 3806-3816.

Guyenet PG & Wang H. (2001). Pre-Bötzinger Neurons With Preinspiratory Discharges "In Vivo" Express NK1 Receptors in the Rat. *Journal of Neurophysiology* **86,** 438-446.

Herlenius E, Lagercrantz H & Yamamoto Y. (1997). Adenosine modulates inspiratory neurons and the respiratory pattern in the brainstem of neonatal rats. *Pediatr Res* **42,** 46-53.

Horner RL. (2012). Neural control of the upper airway: integrative physiological mechanisms and relevance for sleep disordered breathing. *Compr Physiol* **2,** 479-535.

Huxtable AG, Zwicker JD, Alvares TS, Ruangkittisakul A, Fang X, Hahn LB, Posse de Chaves E, Baker GB, Ballanyi K & Funk GD. (2010). Glia Contribute to the Purinergic Modulation of Inspiratory Rhythm-Generating Networks. *J Neurosci* **30,** 3947-3958.

Huxtable AG, Zwicker JD, Poon BY, Pagliardini S, Vrouwe SQ, Greer JJ & Funk GD. (2009). Tripartite Purinergic Modulation of Central Respiratory Networks during Perinatal Development: The Influence of ATP, Ectonucleotidases, and ATP Metabolites. *Journal of Neuroscience* **29,** 14713-14725.

Kasymov V, Larina O, Castaldo C, Marina N, Patrushev M, Kasparov S & Gourine AV. (2013). Differential sensitivity of brainstem versus cortical astrocytes to changes in pH reveals functional regional specialization of astroglia. *J Neurosci* **33,** 435-441.

Koos BJ & Maeda T. (2001). Adenosine A(2A) receptors mediate cardiovascular responses to hypoxia in fetal sheep. *Am J Physiol Heart Circ Physiol* **280,** H83-89.

Koos BJ, Maeda T & Jan C. (2001). Adenosine A(1) and A(2A) receptors modulate sleep state and breathing in fetal sheep. *J Appl Physiol (1985)* **91,** 343-350.

Liu B, Paton JF & Kasparov S. (2008). Viral vectors based on bidirectional cell-specific mammalian promoters and transcriptional amplification strategy for use in vitro and in vivo. *BMC Biotechnol* **8,** 49.

Lorier AR, Huxtable AG, Robinson DM, Lipski J, Housley GD & Funk GD. (2007). P2Y1 Receptor Modulation of the Pre-Botzinger Complex Inspiratory Rhythm Generating Network In Vitro. *J Neurosci* **27,** 993-1005.

Lorier AR, Lipski J, Housley GD, Greer JJ & Funk GD. (2008). ATP sensitivity of preBötzinger complex neurones in neonatal rat in vitro: mechanism underlying a P2 receptor-mediated increase in inspiratory frequency. *The Journal of Physiology* **586,** 1429-1446.

Lorier AR, Peebles K, Brosenitsch T, Robinson DM, Housley GD & Funk GD. (2004). P2 receptors modulate respiratory rhythm but do not contribute to central CO2 sensitivity in vitro. *Respir Physiol Neurobiol* **142,** 27-42.

Monnier A, Alheid GF & McCrimmon DR. (2003). Defining ventral medullary respiratory compartments with a glutamate receptor agonist in the rat. *J Physiol* **548,** 859-874.

Moss IR. (2000). Respiratory responses to single and episodic hypoxia during development: mechanisms of adaptation. *Respir Physiol* **121,** 185-197.

North RA. (2002). Molecular physiology of P2X receptors. *Physiol Rev* **82,** 1013-1067.

Paxinos G & Watson C. (2007). *The rat brain in stereotaxic coordinates*. Academic Press/Elsevier, Amsterdam ; Boston ;.

Prabhakar NR. (2000). Oxygen sensing by the carotid body chemoreceptors. *Journal of Applied Physiology* **88,** 2287-2295.

Rajani V, Zhang Y, Revill AL & Funk GD. (2015). The role of P2Y receptor signaling in central respiratory control. *Respir Physiol Neurobiol***,** In press.

Ramirez JM, Quellmalz UJ & Richter DW. (1996). Postnatal changes in the mammalian respiratory network as revealed by the transverse brainstem slice of mice. *The Journal of physiology* **491 (Pt 3),** 799-812.

Ruangkittisakul A, Panaitescu B, Secchia L, Bobocea N, Kantor C, Kuribayashi J, Iizuka M & Ballanyi K. (2012). Anatomically "Calibrated" Isolated Respiratory Networks from Newborn Rodents. In *Isolated Central Nervous System Circuits*, ed. Ballanyi K, pp. 61-124. Humana Press, Totowa, NJ.

Ruangkittisakul A, Schwarzacher SW, Secchia L, Ma Y, Bobocea N, Poon BY, Funk GD & Ballanyi K. (2008). Generation of eupnea and sighs by a spatiochemically organized inspiratory network. *J Neurosci* **28,** 2447-2458.

Ruangkittisakul A, Schwarzacher SW, Secchia L, Poon BY, Ma Y, Funk GD & Ballanyi K. (2006). High sensitivity to neuromodulator-activated signaling pathways at physiological [K+] of confocally imaged respiratory center neurons in on-line-calibrated newborn rat brainstem slices. *The Journal of neuroscience : the official journal of the Society for Neuroscience* **26,** 11870-11880.

Sak K & Illes P. (2005). Neuronal and glial cell lines as model systems for studying P2Y receptor pharmacology. *Neurochemistry international* **47,** 401-412.

Simon J, Webb TE, King BF, Burnstock G & Barnard EA. (1995). Characterisation of a recombinant P2Y purinoceptor. *European journal of pharmacology* **291,** 281-289.

Smith J, Ellenberger H, Ballanyi K & Richter D. (1991). Pre-Botzinger complex: a brainstem region that may generate respiratory rhythm in mammals. *Science*.

So EL. (2008). What is known about the mechanisms underlying SUDEP? *Epilepsia* **49 Suppl 9,** 93-98.

Spitzer M, Wildenhain J, Rappsilber J & Tyers M. (2014). BoxPlotR: a web tool for generation of box plots. *Nat Methods* **11,** 121-122.

Tang F, Lane S, Korsak A, Paton JFR, Gourine AV, Kasparov S & Teschemacher AG. (2014). Lactate-mediated glia-neuronal signalling in the mammalian brain. *Nat Commun* **5,** 3284.

Teppema LJ & Dahan A. (2010). The ventilatory response to hypoxia in mammals: mechanisms, measurement, and analysis. *Physiol Rev* **90,** 675-754.

Thomas T, Ralevic V, Bardini M, Burnstock G & Spyer KM. (2001). Evidence for the involvement of purinergic signalling in the control of respiration. *Neuroscience* **107,** 481-490.

von Kugelgen I & Wetter A. (2000). Molecular pharmacology of P2Y-receptors. *Naunyn-Schmiedeberg's archives of pharmacology* **362,** 310-323.

Wilson CG, Martin RJ, Jaber M, Abu-Shaweesh J, Jafri A, Haxhiu MA & Zaidi S. (2004). Adenosine A2A receptors interact with GABAergic pathways to modulate respiration in neonatal piglets. *Respir Physiol Neurobiol* **141,** 201-211.

Zwicker JD, Rajani V, Hahn LB & Funk GD. (2011). Purinergic modulation of preBötzinger complex inspiratory rhythm in rodents: the interaction between ATP and adenosine. *J Physiol* **589,** 4583-4600.

ADDITIONAL INFORMATION

Funding

The authors declare no competing financial interests. This work was supported by the Canadian Institutes for Health Research (CIHR, 53085 to GDF, GSD-121789 to VR), National Sciences and Engineering Research Council (NSERC, 402532 to GDF; 435843 to SP), Alberta Innovates Health Solutions (AIHS), University Hospital Foundation (KB) Women and Children's Health Research Foundation, Canadian Foundation for Innovation (CFI), Alberta Science and Research Authority (ASRA) the Wellcome Trust (Grants 095064 and 200893 to AVG), and BBSRC (MR/L020661/1 and BB/L019396/1 to SK) and by the Intramural Research Program of the NIH, NINDS (SSB). (SSB is a NIH-UCL GPP fellow).

FIGURE CAPTIONS

Figure 1: Purinergic modulation of respiratory rhythm: a working hypothesis.
At the synapse of two preBötC inspiratory neurons, volleys of action potentials during inspiration in the presynaptic neuron evoke glutamate release, exciting postsynaptic neurons via ionotropic (GluR) and metabotropic (mGluR) receptors on preBötC inspiratory neurons. During hypoxia, astrocytes sense changes in O_2, causing increases in intracellular calcium (i), resulting in the exocytotic release of gliotransmitters, including ATP (ii). ATP acts via $P2Y_1$ receptors located on preBötC neurons (iii), causing a release of Ca^{2+} from intracellular stores mediated by DAG/IP_3 (iv), and the modulation of downstream ion channels, $[Ca^{2+}]_i$, or the activation of protein kinase C (PKC) (v). Autocrine/paracrine of astrocytes by ATP may also contribute (vi).

Figure 2: Expression of tetanus toxin light chain (TeLC) protein in medullary astrocytes attenuates the hypoxic ventilatory response.
A) Representative recordings obtained in naïve control and TeLC-expressing animals

showing changes in integrated phrenic nerve activity (∫PN), instantaneous frequency (inst. freq., breaths per min, BPM) and blood pressure during 5.5 min of exposure to 10% O_2. B) Time courses of relative frequency, integrated phrenic nerve amplitude (∫PNA) and ventilatory output (frequency × ∫PNA) calculated for the three groups: naïve controls (n=10), viral controls (n=6) expressing eGFP in astroglia, and rats expressing eGFP and TeLC in astroglia (n=6). Phases I and II of the HVR are shaded in grey. C) Comparisons of phase I and II parameters across the three groups reveals a significant decrease in ventilatory output of TeLC expressing rats during both phases I and II ($p<0.5$, One-way ANOVA, Tukey post-hoc test).

Figure 3: Viral expression was centered at the level of the preBötC and limited to astrocytes. A) Schematic showing relative location of peak viral expression with respect to the preBötC in adult rats targeted with AVV-sGFAP-eGFP-TeLC. Inferior olive dorsal (IOD), inferior olive medial (IOM), inferior olive principal (IOP), 4th ventricle (IV), nucleus ambiguus (NA), pyramidal tract (PY), rostral ventrolateral medulla (RVL), spinal trigeminal tract (Sp5), spinal trigeminal interpolar (Sp5I), solitary tract (Sol). Viral expression was centered in the preBötC and dropped off substantially 500 µM rostral and caudal to the injection site that was centered in the preBötC. B) The region expressing TeLC-eGFP adenovirus is centered in the region containing a high density of NK1 receptor expressing neurons, are present in. C) Double-labeling of cells with the neuronal marker NeuN and the glial specific AAV, detected via eGFP, was not detected. Ten NeuN labeled cells are circled to facilitate comparison between images).

Figure 4: Functional identification of preBötC via microinjections of DLH. Unilateral injection of DLH (10 mM) into the VLM of urethane-anesthetized, paralyzed adult rats while measuring instantaneous respiratory frequency (inst. freq.) from phrenic nerve activity (∫PN). A) Unilateral injection of DLH into the preBötC produces a robust increase in respiratory frequency. B) Injection of DLH 200 µm rostral to the preBötC (presumably

in the BötC) reduced inspiratory frequency. C) DLH injection 300 µm caudal to the preBötC had minimal effect on inspiratory rhythm.

Figure 5: Activation of $P2Y_1$ receptors in the preBötC of adult rat in vivo with MRS 2365 (1 mM) evokes an increase in respiratory frequency and a decrease in tidal volume (V_T) A) Airflow and diaphragm (DIA) EMG recordings show the response of an adult anesthetized vagotomized rat to unilateral injection of MRS 2365 (1mM, 200nl) into the preBötC. B) Time course of instantaneous frequency (inst. freq.), V_T, and minute ventilation ($\dot{V}_E$) responses evoked by a single injection of MRS 2365. C) Group data (n=8) illustrating the change in frequency, V_T and $\dot{V}_E$ relative to control (* indicates significant different from predrug control values , $p< 0.05$, paired t- test). D) Schematic showing 8 injection sites. Inferior olive dorsal (IOD), inferior olive medial (IOM), inferior olive principal (IOP), 4th ventricle (IV), nucleus ambiguous (NA), pyramidal tract (PY), rostral ventrolateral medulla (RVL), spinal trigeminal tract (Sp5), spinal trigeminal interpolar (Sp5I), solitary tract (Sol).

Figure 6: Adenosine (500 µM) microinjected into the preBötC of adult rat in vivo has no effect on respiratory frequency or tidal volume (V_T). A) Airflow, diaphragm (DIA) and genioglossus (GG) EMG recordings show the response of an adult anesthetized vagotomized rat to unilateral injection of adenosine into the preBötC. B) Airflow, diaphragm (DIA) and genioglossus (GG) EMG recordings show the response of an adult anesthetized vagotomized rat to injection of DLH (1 mM) into the preBötC**.** C) Group data illustrating the change in frequency and V_T relative to control (n=8) (* indicates significant difference from predrug controls values, (paired t-test $P< 0.05$). D) Schematic showing 8 injection sites in relation to inferior olive dorsal (IOD), inferior olive medial (IOM), inferior olive principal (IOP), 4th ventricle (IV), nucleus ambiguus (NA), pyramidal tract (PY), rostral ventrolateral medulla (RVL), spinal trigeminal tract (Sp5), spinal trigeminal interpolar (Sp5I), solitary tract (Sol). E) Tissue section showing injection site marked with fluorescent microspheres (yellow). PreBötC neurons ($NK1^+$) are present in the region of the injection site.

Figure 7: Unilateral inhibition of $P2Y_1$ receptors in the preBötC of adult paralyzed rats in vivo with MRS 2279 increases the secondary hypoxic respiratory depression. A) Representative traces showing changes in integrated phrenic nerve activity (∫PN) and instantaneous frequency (inst. freq. BPM) evoked by exposure to 5 min of 10% O_2 following injection of vehicle (HEPES) or MRS 2279 into the preBötC. B) *(Left)* Time courses of relative frequency, integrated phrenic nerve amplitude (∫PNA) and ventilatory output (frequency × ∫PNA) calculated before and after injection of MRS 2279 (n=6). Phases I and II of the HVR are shaded in grey. *(Right)* Comparisons of phase I and II parameters between vehicle and MRS 2279 responses (* indicates significant difference between control (HEPES) and MRS 2279 trials $p < 0.5$, paired t-test). C) Schematic showing 6 injection sites. Inferior olive dorsal (IOD), inferior olive medial (IOM), inferior olive principal (IOP), 4th ventricle (IV), nucleus ambiguus (NA), pyramidal tract (PY), rostral ventrolateral medulla (RVL), spinal trigeminal tract (Sp5), spinal trigeminal interpolar (Sp5I), solitary tract (Sol).

Figure 8: The hypoxic ventilatory response does not change with repeated exposure; time-matched controls. A) Representative traces from the same animal showing changes in integrated phrenic nerve activity (∫PN) and instantaneous frequency (inst. freq., BPM) during two consecutive hypoxic exposures (1 hour apart) following stereotaxic injection of vehicle (HEPES) into the preBötC. B) *(Left)* Time courses of relative frequency, integrated phrenic nerve amplitude (∫PNA) and ventilatory output (frequency × ∫PNA) calculated before and after injection of MRS 2279 (n=6). Phases I and II of the HVR are shaded in grey. *(Right)* The phase I and II components of the HVR were similar during consecutive exposure to hypoxia under control conditions (i.e., after HEPES injection)($p > 0.5$, paired t-test).

Figure 9: Increases in $[Ca^{2+}]_i$ contribute to the $P2Y_1$ receptor mediated frequency increase in vitro. A) Representative traces of integrated hypoglossal nerve output (∫XII) evoked in response to $P2Y_1$ agonist MRS 2365 (10s, 100 μM) before and after the local application of the cell permeable calcium chelator EGTA-AM (1 mM) to the preBötC. B) Box plot summarizing group data (n = 6, p = 0.0047, paired t-test). C) Representative traces

∫XII nerve output evoked in response to MRS 2365 (10s, 100 μM) in control and after local application of thapsigargin (30 min, 200 μM). D) Box plot summarizing group data (n= 6 , p=0.007, paired t-test). Time matched control experiments showed no significant effect on the MRS 2365 response of locally applying vehicle (0.2% DMSO) into the preBötC for 30 minutes of (n=5, p>0.05, paired t-test).

Figure 10: Activation of $P2Y_1$ receptors on preBötC inspiratory neurons in vitro evokes a thapsigargin-sensitive, increase in $[Ca^{2+}]_i$. A) Multiphoton images of baseline Fluo-4 fluorescence indicating $[Ca^{2+}]_i$ in 5 inspiratory neurons at a single optical plain (top), inspiratory-related oscillations in $[Ca^{2+}]_i$ and the peak $[Ca^{2+}]_i$ increase evoked in response to locally applied MRS 2365 (100 μM, 10 s) (bottom) B) $[Ca^{2+}]_i$ increases in the neurons of (A) are synchronous with ∫XII and their responses to locally applied MRS 2365 (100 μM, 10 s). C) Group data showing an approximate 50% increase in peak Fluo-4 fluorescence in response to local application of MRS 2365 (100 μM, 10 s) over inspiratory preBötC neurons (n=18, 5 slices, p <0.0001, paired t-test); A.U., arbitrary units. D) Multiphoton images of Fluo-4 Ca^{2+} fluorescence in 2 inspiratory neurons at a single optical plain at baseline (top), at the peak of two control MRS 2365-evoked (10 μM, 1 min, bath application) Ca^{2+} fourescence responses (top middle, bottom middle), seperated by 30 minute intervals. The bottom image shows the response evoked by MRS 2365 after bath application of thapsigargin (100 μM, 30 min). E) Traces of Fluo-4 Ca^{2+} flourescent responses evoked by MRS2365 in the same neurons shown in (D). F) Group data comparing the decrease in peak MRS 2365 evoked Fluo-4 Ca^{2+} response that occurred between control response 1 and 2 with the decrease in the MRS 2365 evoked Ca^{2+} response that occurred between the second control MRS 2365 response and the MRS 2365 response in thapsigargin/CPA (n=12, p<0.0001, paired t-test).

Figure 11: Responses of cultured preBötC glia to ATP are sensitive to depletion of intracellular calcium stores. A) Images showing a phase contrast image of cultured glia (far left panel), and fluo-4 Ca^{2+} fourescence under baseline conditions (middle-left panel), during local application of ATP (100 μM, 10 s,) (middle-right panel), and during local

application of ATP after pre-application of SERCA inhibitor thapsigargin (50 nm, 30 min) (far right panel). B) Time course of ATP-evoked fluorescence changes measured from 4 ROIs (numbered in A) in control (left), and after thapsigargin application (middle). Group data (n=54) showing relative changes in fluorescence ($F_{peak}/F_{baseline}$) in response to ATP and to ATP in the presence of thapsigargin (right) reveal that thapsigargin significantly reduced the ATP-evoked increase in Ca^{2+} fluorescence (n=53, $p<0.001$, paired t-test).

Figure 12: Effect of CNQX and AP5/MK-801 on ATP currents evoked in preBötC inspiratory neurons in TTX.

A) Representative traces showing an ATP current evoked in an inspiratory preBotC neuron in a rhythmic slice (note inspiratory synaptic currents pre-TTX), after TTX and again in TTX after bath application of CNQX (10 μM) and AP5 (100 μM). B) Group data comparing the relative reduction in the ATP current that occurs with consecutive applications in a time matched-control group (n=6) with reduction that was produced by CNQX+AP5/MK-801 group (n=8). CNQX and AP5/MK-801 did not affect the amplitude of ATP-induced inward currents ($p>0.05$, unpaired t-test).

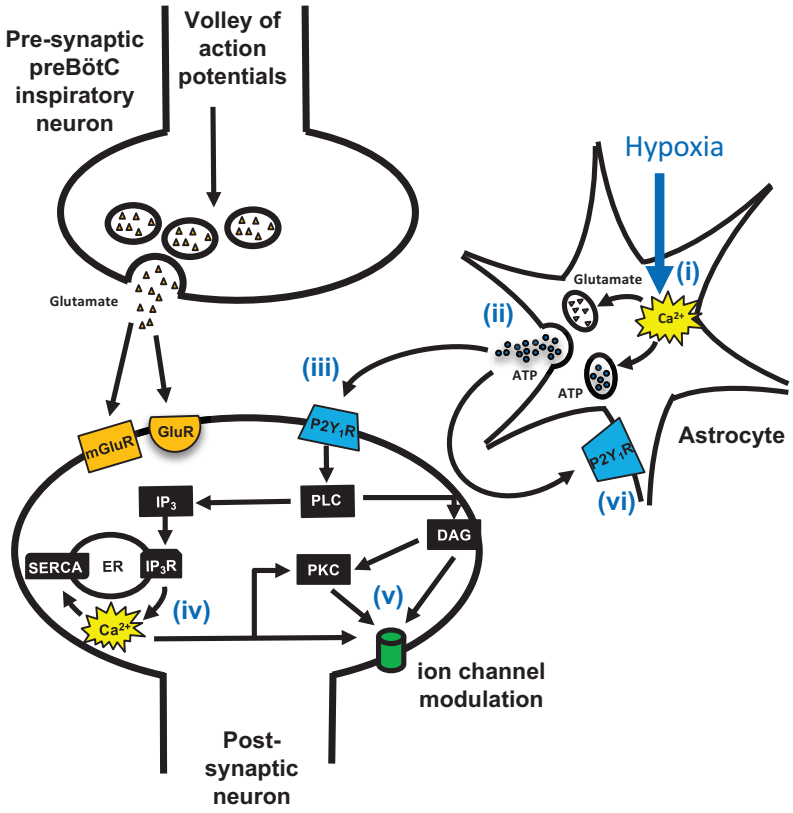
Pre-synaptic preBötC inspiratory neuron
Volley of action potentials
Glutamate
Hypoxia
Glutamate
(i)
Ca2+
(ii)
ATP
ATP
(iii)
Astrocyte
mGluR
GluR
P2Y1R
P2Y1R
(vi)
IP3
PLC
DAG
SERCA
ER
IP3R
PKC
(v)
Ca2+
(iv)
ion channel modulation
Post-synaptic neuron

Figure 1

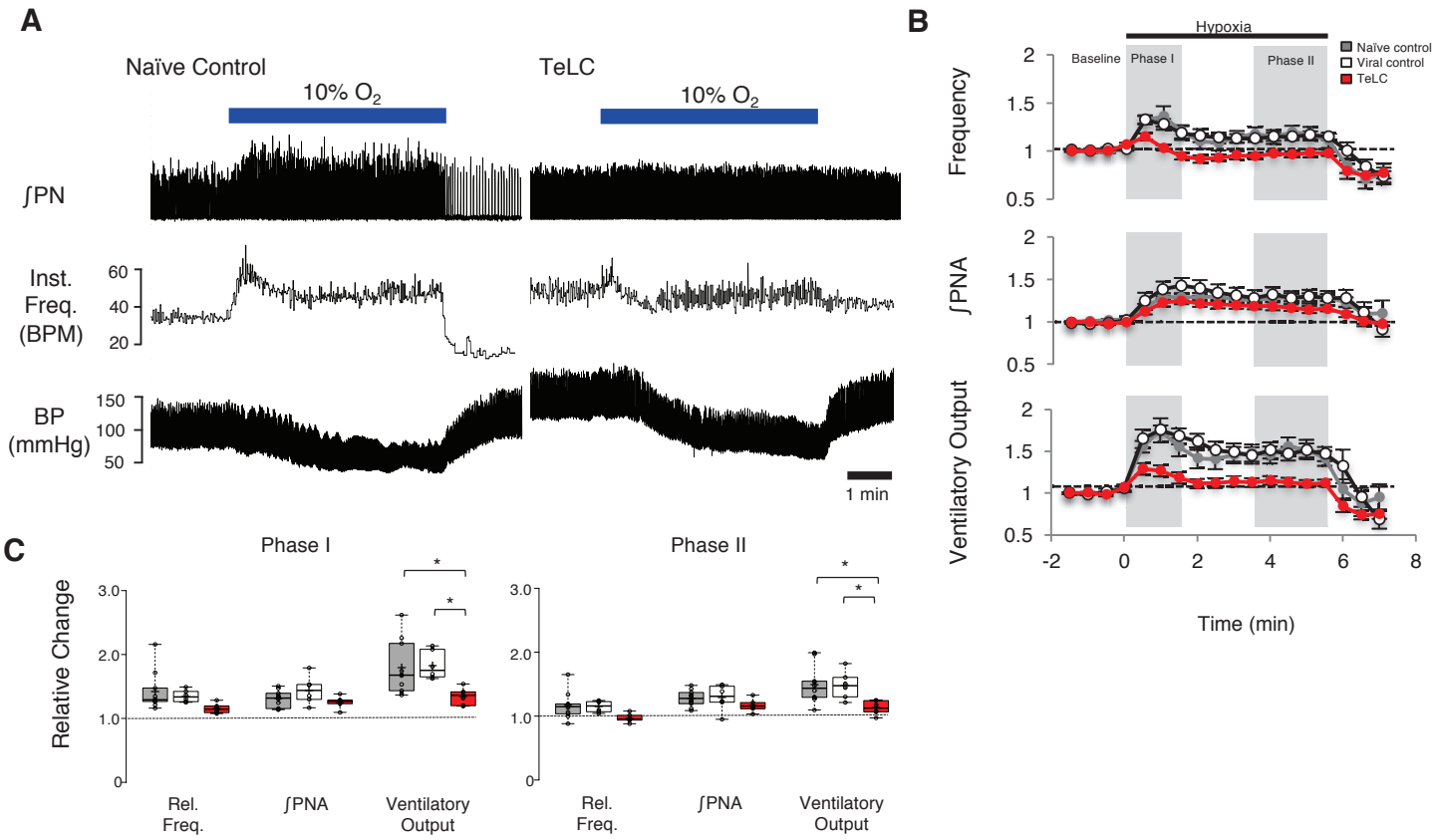
A
Naïve Control
TeLC
10% O2
10% O2
∫PN
Inst. Freq. (BPM)
60
40
20
BP (mmHg)
150
100
50
1 min
B
Hypoxia
Baseline
Phase I
Phase II
Naïve control
Viral control
TeLC
Frequency
∫PNA
Ventilatory Output
2
1.5
1
0.5
-2
0
2
4
6
8
Time (min)
C
Phase I
Phase II
Relative Change
3.0
2.0
1.0
0
Rel. Freq.
∫PNA
Ventilatory Output

Figure 2

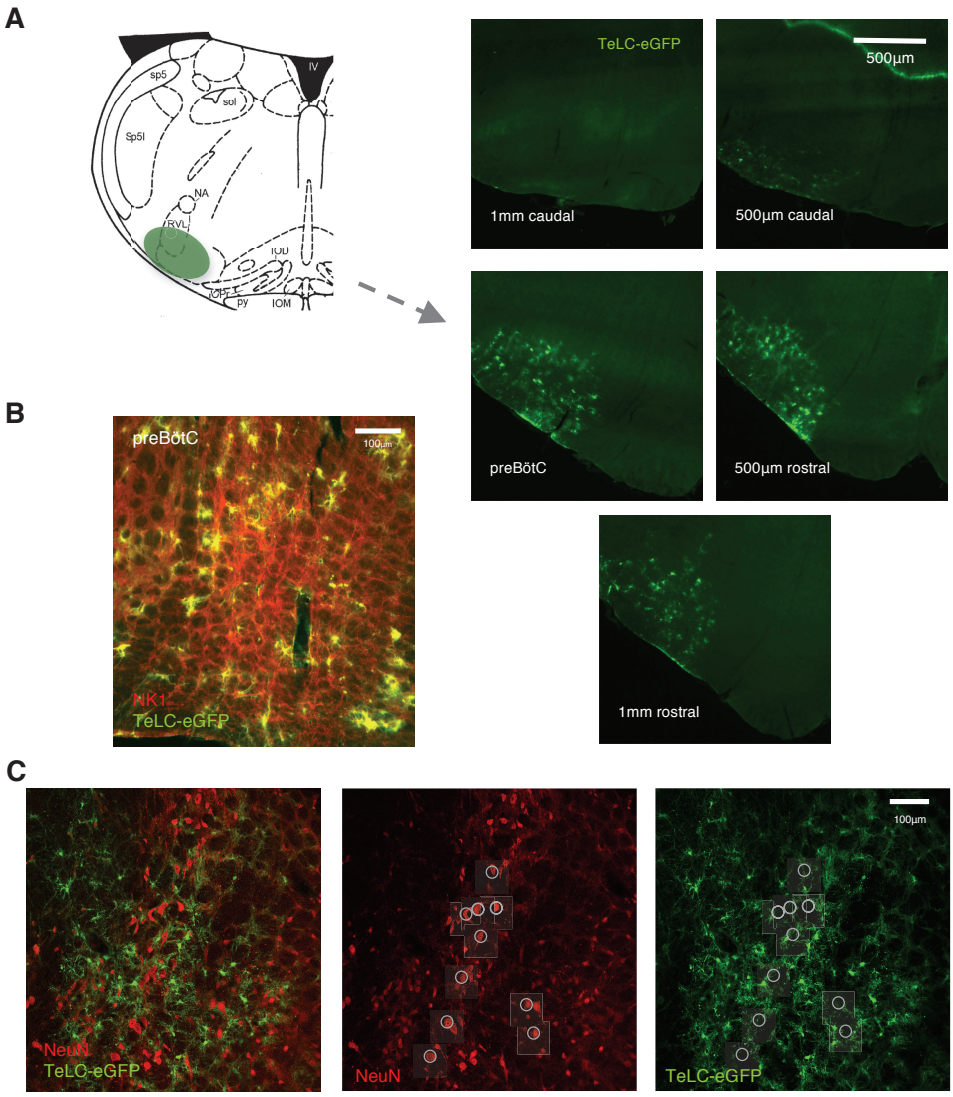
A
sp5
IV
sol
Sp5I
NA
RVL
py
IOM
TeLC-eGFP
500µm
1mm caudal
500µm caudal
preBötC
500µm rostral
1mm rostral
B
preBötC
100µm
NK1
TeLC-eGFP
C
NeuN
TeLC-eGFP
NeuN
100µm
TeLC-eGFP

Figure 3

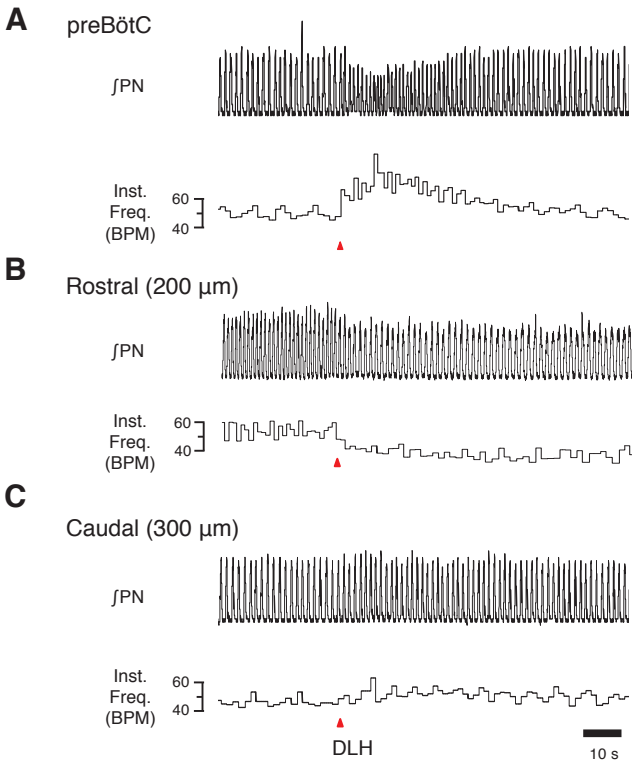
A
preBötC
∫PN
Inst.
Freq.
(BPM)
60
40
B
Rostral (200 µm)
∫PN
Inst.
Freq.
(BPM)
60
40
C
Caudal (300 µm)
∫PN
Inst.
Freq.
(BPM)
60
40
DLH
10 s

Figure 4

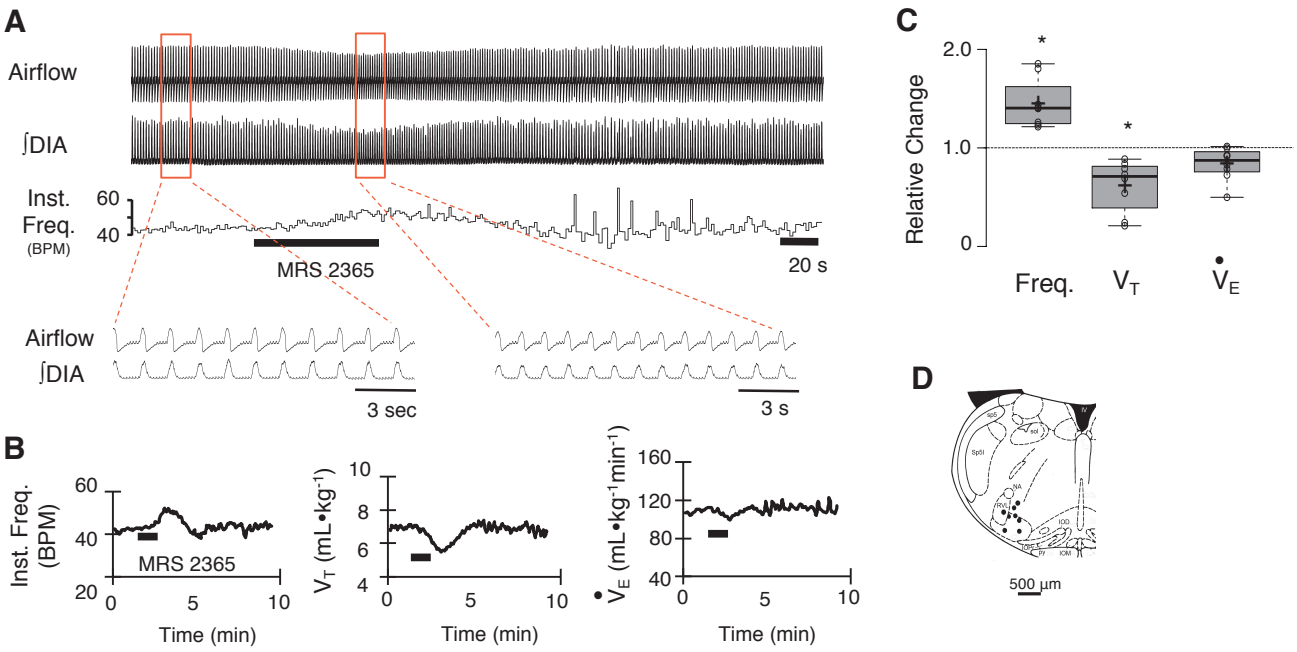
A
Airflow
∫DIA
Inst. Freq. (BPM)
60
40
MRS 2365
20 s
Airflow
∫DIA
3 sec
3 s
C
Relative Change
2.0
1.0
0
Freq.
V_T
$\dot{V}_E$
B
Inst. Freq. (BPM)
MRS 2365
Time (min)
V_T (mL•kg^{-1})
Time (min)
$\dot{V}_E$ (mL•kg^{-1}min^{-1})
Time (min)
D
500 µm

Figure 5

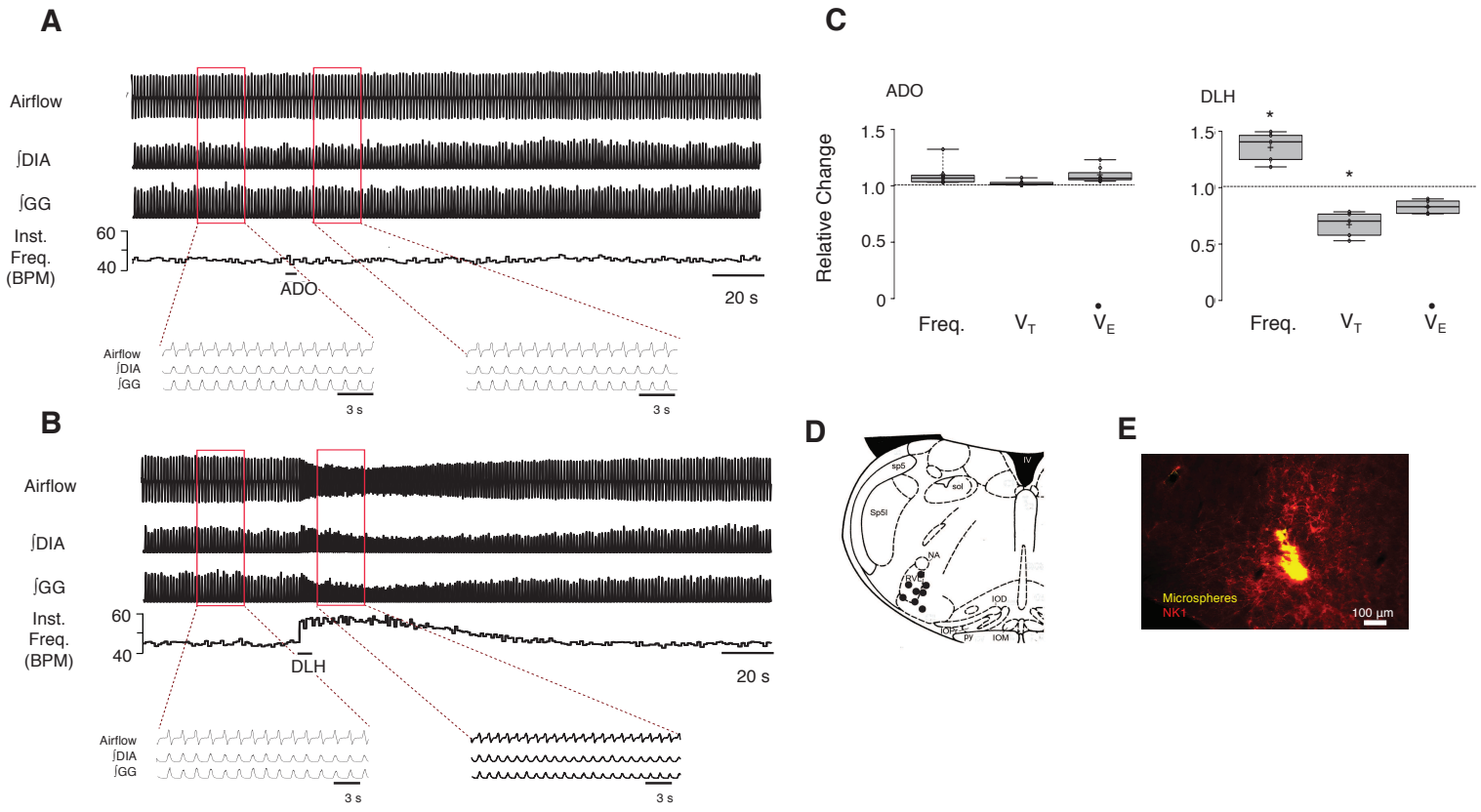
A
Airflow
∫DIA
∫GG
Inst. Freq. (BPM)
60
40
ADO
20 s
Airflow
∫DIA
∫GG
3 s
3 s
B
Airflow
∫DIA
∫GG
Inst. Freq. (BPM)
60
40
DLH
20 s
Airflow
∫DIA
∫GG
3 s
3 s
C
ADO
DLH
Relative Change
1.5
1.0
0.5
0
Freq.
V_T
$\dot{V}_E$
*
*
D
spS
sol
IV
SpSl
NA
RVL
IOD
IOS
py
IOM
E
Microspheres
NK1
100 µm

Figure 6

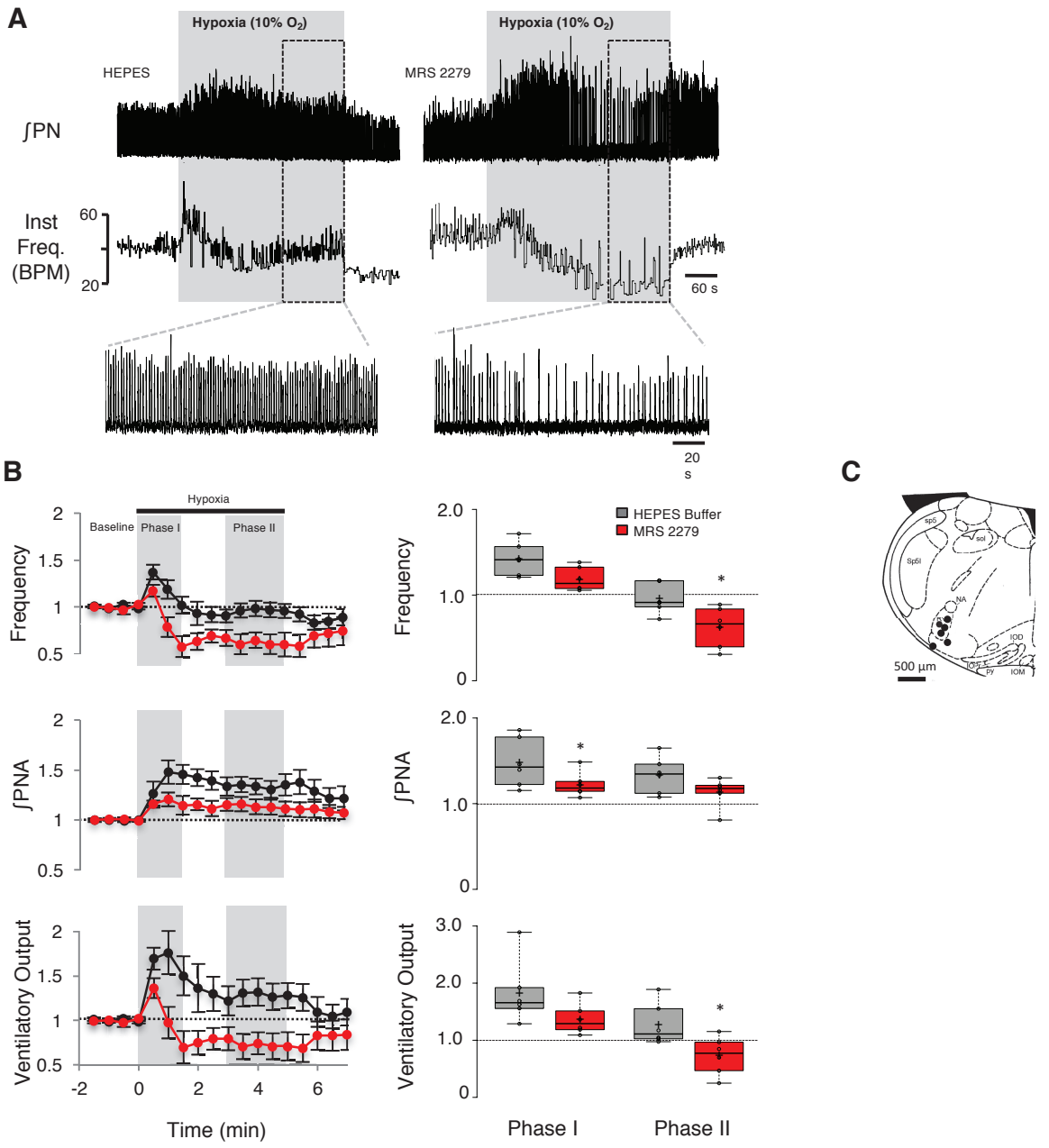
A
Hypoxia (10% O2)
Hypoxia (10% O2)
HEPES
MRS 2279
∫PN
Inst Freq. (BPM)
60
20
60 s
20 s
B
Hypoxia
Baseline
Phase I
Phase II
Frequency
∫PNA
Ventilatory Output
Time (min)
HEPES Buffer
MRS 2279
Phase I
Phase II
C
500 µm

Figure 7

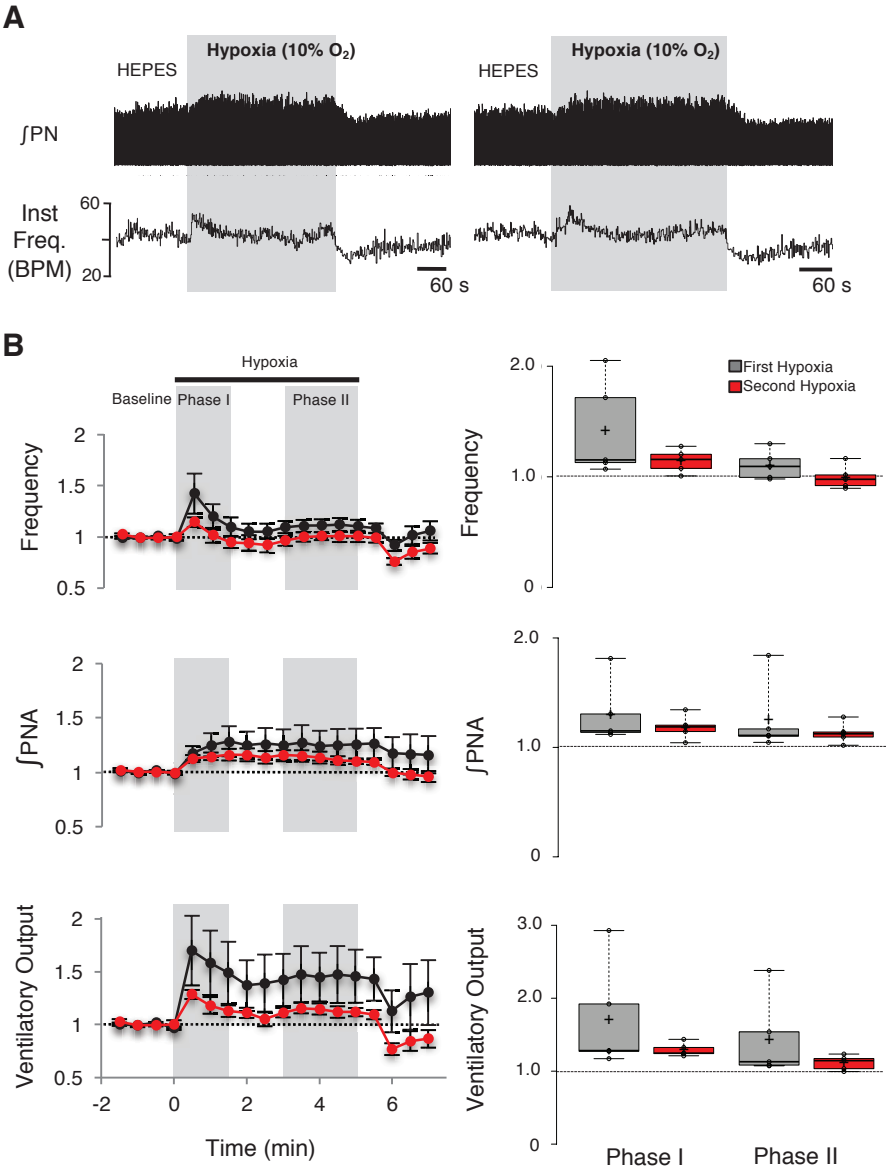
A
HEPES
Hypoxia (10% O2)
HEPES
Hypoxia (10% O2)
∫PN
Inst Freq. (BPM)
60
20
60 s
60 s
B
Hypoxia
Baseline
Phase I
Phase II
Frequency
∫PNA
Ventilatory Output
Time (min)
First Hypoxia
Second Hypoxia
Phase I
Phase II

Figure 8

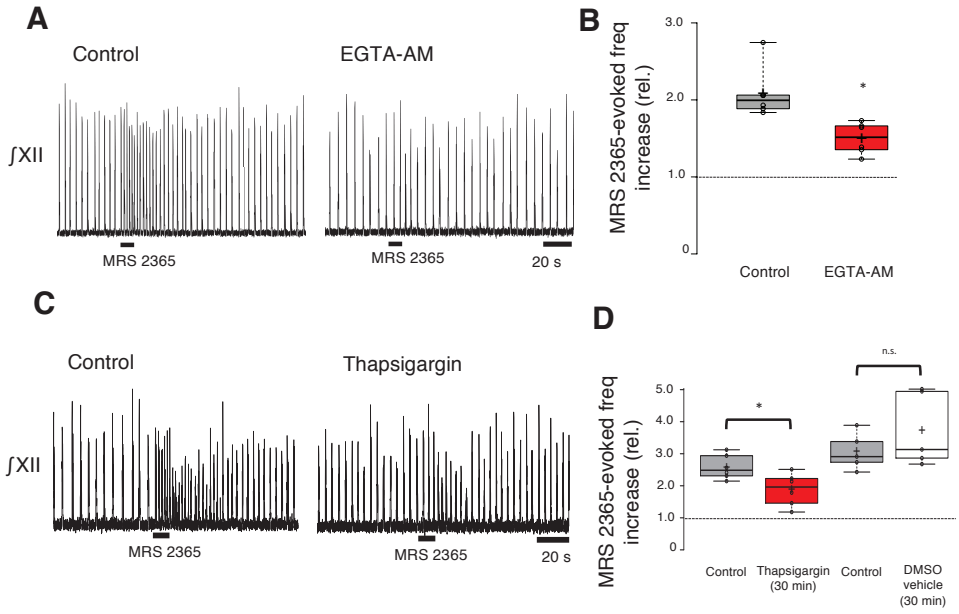
A
Control
EGTA-AM
∫XII
MRS 2365
MRS 2365
20 s
B
MRS 2365-evoked freq increase (rel.)
3.0
2.0
1.0
0
*
Control
EGTA-AM
C
Control
Thapsigargin
∫XII
MRS 2365
MRS 2365
20 s
D
MRS 2365-evoked freq increase (rel.)
5.0
4.0
3.0
2.0
1.0
0
*
n.s.
Control
Thapsigargin (30 min)
Control
DMSO vehicle (30 min)

Figure 9

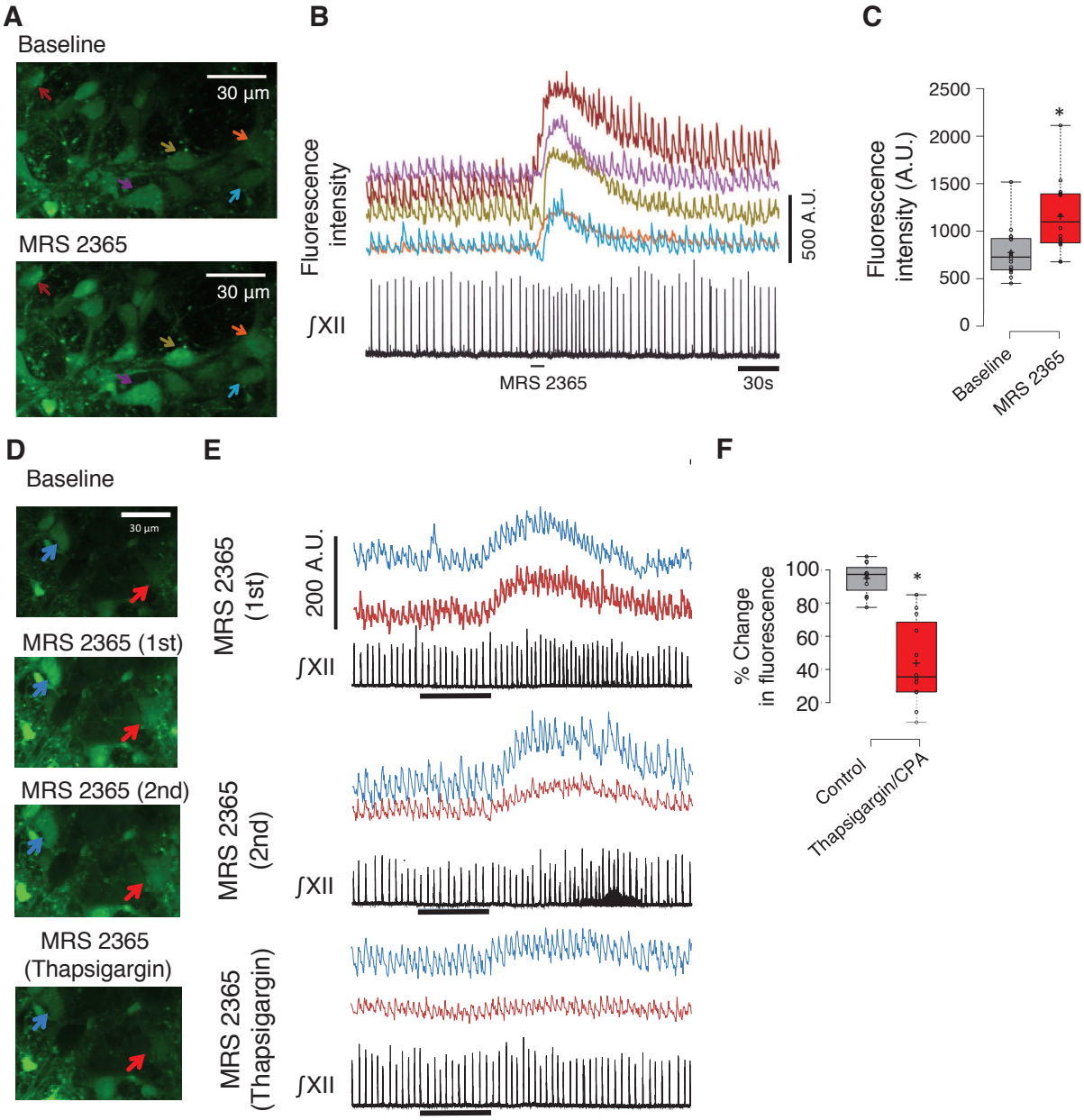
A
Baseline
30 µm
MRS 2365
30 µm
B
Fluorescence intensity
500 A.U.
∫XII
MRS 2365
30s
C
Fluorescence intensity (A.U.)
2500
2000
1500
1000
500
0
*
Baseline
MRS 2365
D
Baseline
30 µm
MRS 2365 (1st)
MRS 2365 (2nd)
MRS 2365 (Thapsigargin)
E
MRS 2365 (1st)
200 A.U.
∫XII
MRS 2365 (2nd)
∫XII
MRS 2365 (Thapsigargin)
∫XII
F
% Change in fluorescence
100
80
60
40
20
*
Control
Thapsigargin/CPA

Figure 10

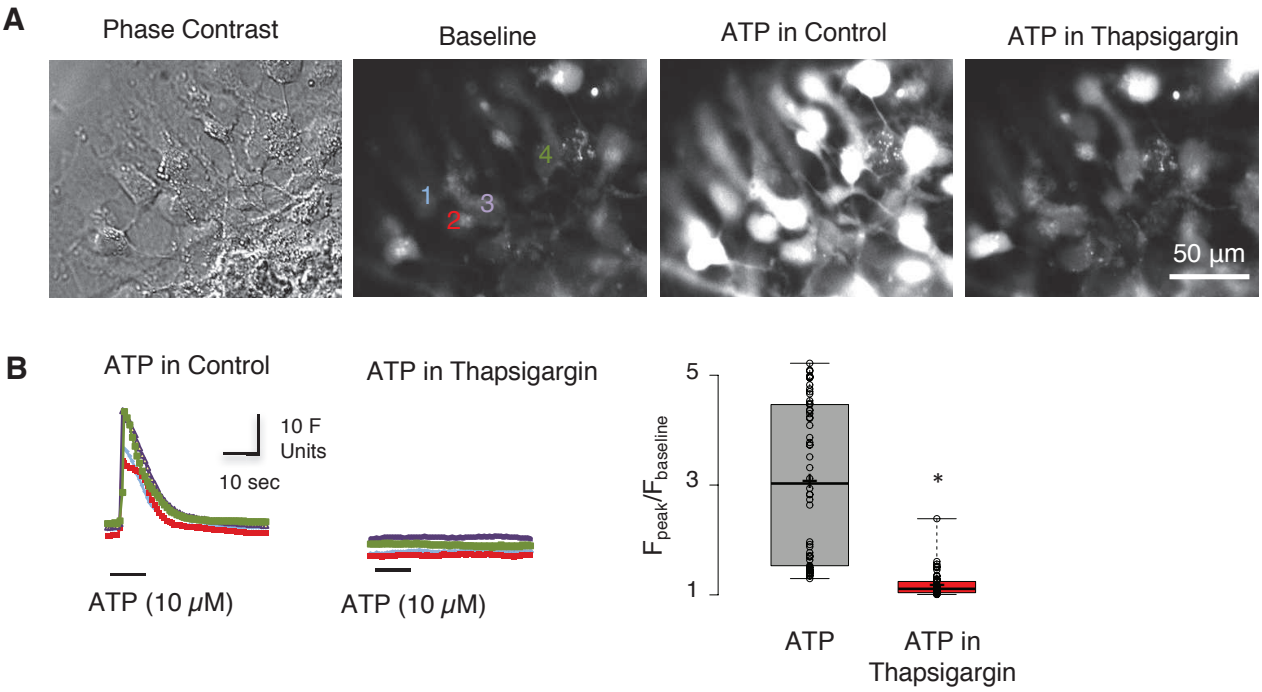
A
Phase Contrast
Baseline
ATP in Control
ATP in Thapsigargin
1
2
3
4
50 µm
B
ATP in Control
ATP in Thapsigargin
10 F
Units
10 sec
ATP (10 µM)
ATP (10 µM)
5
3
1
F peak/F baseline
*
ATP
ATP in
Thapsigargin

Figure 11

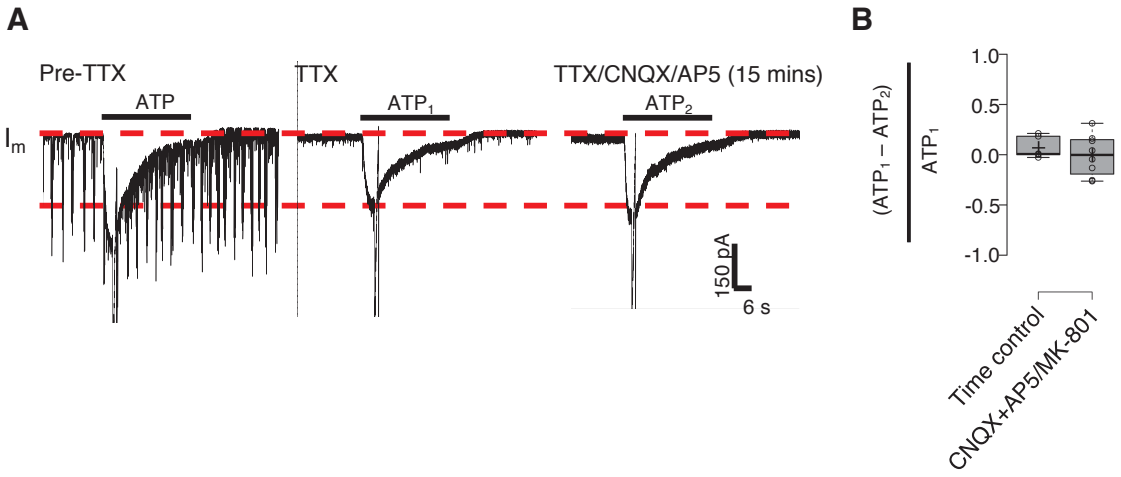
A
Pre-TTX
TTX
TTX/CNQX/AP5 (15 mins)
ATP
ATP1
ATP2
Im
150 pA
6 s
B
(ATP1 – ATP2)
ATP1
1.0
0.5
0.0
-0.5
-1.0
Time control
CNQX+AP5/MK-801

Figure 12